The Anatomical Record

Developmental origins of the crocodylian skull table and platyrostral face

Journal:	*Anatomical Record*
Manuscript ID	AR-SI-Croc-21-0331
Wiley - Manuscript type:	Special Issue Article
Date Submitted by the Author:	09-Aug-2021
Complete List of Authors:	Morris, Zachary; Yale University, Department of Earth and Planetary Sciences Vliet, Kent; University of Florida, Department of Biology Abzhanov, Arhat; Imperial College London, Department of Life Sciences; Natural History Museum Pierce, Stephanie; Harvard University, Department of Organismic and Evolutionary Biology and Museum of Comparative Zoology
Keywords:	Crocodylia, ontogeny, platyrostry, skull shape

Developmental origins of the crocodylian skull table and platyrostral face

Author list:
Zachary S. Morris[1,2], Kent A. Vliet [3], Arhat Abzhanov[4,5], Stephanie E. Pierce[1]

Affiliations:
1. Museum of Comparative Zoology and Department of Organismic and Evolutionary Biology, Harvard University, 26 Oxford Street, Cambridge, MA 02138 USA
2. Current Address: Department of Earth & Planetary Sciences, Yale University, 210 Whitney Avenue, New Haven, CT 06511 USA
3. Department of Biology, University of Florida, 876 Newell Drive, Gainesville, FL 32611, USA
4. Department of Life Sciences, Imperial College London, Silwood Park Campus, Buckhurst Road, Ascot, Berkshire SL5 7PY UK
5. Natural History Museum, Cromwell Road, London SW7 5BD UK

Keywords: Crocodylia, ontogeny, skull shape, platyrostry, developmental constraint

Author Correspondence: zachary.morris@yale.edu; spierce@fas.harvard.edu

Running title: Development of crocodylian cranial flatness

Data availability: All data, code, and results needed to replicate this study are available in the Dryad Digital Repository: https://doi.org/10.5061/dryad.v15dv41wm. Additional supplementary tables can be found in the electronic supplementary materials. CT data and images have been reposited with the museums that hold copyright to the original specimens. Requests to use scan data should be made directly to those institutions.

Funding: Funding was provided by the Department of Organismic and Evolutionary Biology at Harvard University (Z.S.M.), the Society of Vertebrate Paleontology Wood's Award (Z.S.M.), NSF DDIG Award #1701745 (Z.S.M. and S.E.P.), and NSF EAR-PF Award #1952888 (Z.S.M.)

Conflict of interest disclosure: The authors have no competing interests.

Ethics: The majority of specimens used in this study are reposited in accredited museums. Additional embryos were collected following approved methods for reptilian embryos at Harvard University and Imperial College.

Abstract

The dorsoventrally flattened skull typifies extant Crocodylia perhaps more than any other anatomical feature and is generally considered an adaptation for semi-aquatic feeding. Although the evolutionary origins have been extensively studied, the developmental origins of craniofacial flattening have yet to be explored. To understand how the skull table and platyrostral snout develop, we quantified embryonic development and post-hatching growth (ontogeny) of the crocodylian skull in lateral view using geometric morphometrics. Our dataset (n=103) includes all but one extant genus and all of the major ecomorphs, including the extremely slender-snouted *Gavialis* and *Tomistoma*. Our analysis reveals that the embryonic development of the flattened skull is remarkably similar across ecomorphs, including the presence of a conserved initial embryonic skull shape, similar to prior analysis of dorsal snout shape. Although differences during post-hatching ontogeny of the snout are recovered among ecomorphs the embryonic patterns are not distinct, revealing an important shift in developmental rate near hatching. In particular, the flattened skull table is achieved by the end of embryonic development with no changes after hatching. Further, the rotation of skull roof and facial bones during development is critical for the stereotypical flatness of the crocodylian skull. Our results suggest selection on hatchling performance and constraints on embryonic skull shape may have been important in this pattern of developmental conservation. The appearance of aspects of cranial flatness among Jurassic stem crocodylians suggests key aspects of these cranial developmental patterns may have been conserved for over 200 million years.

Introduction

Extant crocodylians (alligators, crocodiles, and gharials) are readily identifiable by their dorsoventrally 'flattened' skulls, a feature generally considered to be an adaptation to aquatic feeding (Langston, 1973; Iordansky, 1973; Brochu, 2001). The crocodylian snout has been the focus of extensive evolutionary and biomechanical research (e.g., Busbey, 1995; McHenry et al., 2006; Pierce et al., 2008; Rayfield & Milner, 2008; Erickson et al., 2012), especially the convergent evolution of similar snout proportions and ecologies (e.g., Brochu, 2001; Pierce et al., 2009). Among living species the spectrum of snout proportions can be roughly divided into three major ecomorphs: 'blunt' forms with short and wide snouts, 'slender' forms with narrow, elongated snouts, and 'moderate' forms in between (Pierce et al., 2008). Unlike the significant variation in snout proportions, the distinctively 'compressed' skull is relatively conserved across crocodylians (see McHenry et al., 2006). This uniquely flat cranial form can be split into three main components: 1) the platyrostral snout at the front of the face; 2) the laterally expanded and flat skull roof or skull table above the braincase; and 3) the laterally flared jaw joint. This contrasts with the undoubtedly ancestral oreinirostral skull condition typical of stem archosaurs and early pseudosuchians, which is characterized by vertically oriented facial elements and a more laterally open skull roof (Busbey, 1995). These striking differences in cranial anatomy have naturally led to questions about the mechanisms underlying such evolutionary transformations.

It has been suggested that platyrostral snouts may help resist axial torsion (e.g., Langston, 1973; Busbey, 1995) during the classic 'death roll' or twist feeding behavior common to crocodylians (Drumheller et al., 2019). However, biomechanical analyses show oreinirostral faces are almost always better at distributing stresses (McHenry et al., 2006; Rayfield & Milner, 2008) and features such as the extensive overlap of bones ('scarf joints'), pterygoid buttressing of the mandible, and the complete secondary palate are mechanisms to overcome the structural weakness of a flattened snout (McHenry et al., 2006). Thus, a complex interaction of selection for hydrodynamic performance and feeding is hypothesized to have driven the evolution of several aspects of snout and skull form, including platyrostry (Cleuren and Vree, 2000; McHenry et al., 2006; Pierce et al., 2008; Pierce et al., 2009). The fossil record provides further evidence, as relatively compressed and elongated snouts have evolved multiple times among aquatic archosaurs (e.g., Stocker & Butler, 2013) and are strongly correlated with increasing aquatic specialization during crocodyliform evolution (Wilberg et al., 2019). In fact, the origin of modern crocodylian platyrostry appears to be optimized in most phylogenetic analyses near the base of Neosuchia (Rayfield & Milner, 2008; Pol et al., 2013) alongside a shift toward semi-aquatic habitats (Wilberg et al., 2019). These different lines of evidence strongly suggest that the evolution of the crocodylian snout has been heavily influenced by selective pressures found in aquatic habitats.

The evolution of the skull table and how it contributes to the flatness of the crocodylian skull have been less thoroughly explored, despite being included in several phylogenetic datasets (e.g., Pol et al., 2013; Narváez et al., 2016; Wilberg et al., 2019). The skull table is in close physical proximity with the brain, neck musculature, and the ear, which indicate that the origin of a crocodylian-like skull table likely had critical implications for many aspects of ecology among stem crocodylians (e.g., Montefeltro et al., 2016). In particular, the lateral edge of the skull table which falls along the squamosal-postorbital bar supports the dorsal earflap and overlies the tympanic recess (Shute & Bellairs, 1955; Iordansky, 1973), thereby greatly affecting the shape of the crocodylian external ear. Intriguingly, an expanded and flattened skull table seems to be present among terrestrial stem crocodylians by the Late Triassic (e.g., Pol et al., 2013), prior to the origin of platyrostry. The differences in the temporal and environmental contexts for the origins of platyrostral snouts and skull tables suggests that each region may have been subject to distinct selective forces and functional constraints, despite both being associated with the flatness of extant crocodylian skulls.

One area which has the potential to illuminate our understanding of the mechanisms underlying crocodylian cranial evolution is the embryonic development and post-hatching growth,

or ontogeny, of the skull. Previous studies in crocodylians have revealed that development may bias or constrain the evolution of dorsal skull shape, as identical ontogenetic patterns underlie convergence in some species and all ecomorphs share a conserved skull shape as embryos (Piras et al., 2010; Watanabe & Slice, 2014; Morris et al., 2019). However, modification to developmental timing, or heterochrony, was also fundamental for both the divergence and convergence in snout shape among crocodylians (Morris et al., 2019). The interplay among such developmental processes has been shown to play a key role in generating the patterns of disparity observed in many vertebrate clades (e.g., Sanger et al., 2014; Camacho et al., 2020), demonstrating the importance of studying the evolution of ontogeny itself. However, many critical questions about the ontogeny of lateral skull shape in crocodylians have yet to be explored: how conserved are the embryonic origins of lateral skull shape across crocodylian ecomorphs?; what are the major anatomical changes that give rise to the flatness of the crocodylian skull during ontogeny?; do similar developmental mechanisms drive evolution of lateral skull ontogeny as discovered for the dorsal skull? Here, we use geometric morphometrics to quantify the ontogeny of lateral skull shape and the curvature fo the snout and skull table, individually, to address these questions. By exploring the embryonic formation of the lateral skull and capturing ecomorph and species-specific ontogenetic trajectories of shape change, we aim to understand how the uniquely flat crocodylian skull is achieved from embryos to adults and whether the evolution of developmental patterns can provide insight into the mechanisms underlying craniofacial evolution.

Materials & Methods

Specimen selection and imaging

Our dataset (n=103) sampled 9 crocodylian species across embryonic and post-hatching ontogeny (table S1). This sample captured nearly all extant genera (except *Melanosuchus*) and all ecomorphs (table S2), including the extremely slender-snouted *Gavialis gangeticus* and *Tomistoma schlegelii*. Specimens were divided into ontogenetic stages following Morris et al. (2019), including two embryonic (mid-skeletal and late-skeletal stages) and 4 post-hatching stages (hatchling, juvenile, subadult, and adult). Species were also categorized into blunt, moderate, and slender cranial ecomorphs (both with and without *G. gangeticus* and *T. schlegelii*) for comparative analyses to account for unevenness in the sampling ontogenetic stages among individual species. To capture the flattening and reorientation of the skull across ontogeny, specimens were positioned with the palate in the horizontal plane prior to imaging from lateral view using a Nikon D90 digital camera or in VGSTUDIO Max 2.3 (Volume Graphics GmbH, Heidelberg, Germany) for CT scans. In lateral view, the profile of the skull roof, anterodorsal border of the orbit, and lateral aspect of snout are all clearly visible.

CT Scanning

CT scans were generated using the Harvard CNS or Natural History Museum, London micro-CT systems (both X-Tek HMX ST 225) with a Molybdenum target. The ossifying skull bones of alcohol preserved embryos and hatchlings were targeted without any contrast enhancing stains. Scan parameters were set to maximize useful contrast individually for each scan (Data available from the Dryad Digital Repository: doi.org/10.5061/dryad.v15dv41wm). CT scan reconstruction was conducted using CT 3D pro (X-Tek), verifying appropriate reconstruction of center of rotation and cropping projection images. CT scans were imported into VGStudio Max 2.3 (Volume Graphics GmbH, Heidelberg, Germany) for further processing. Using the specific histogram of gray values for each specimen, the opacity of gray values was modulated in order to minimize non-skeletal materials (air, ethanol filled soft-tissue) and noise. Segmenting of bony elements, and identification of the position and edges of developing bone, was done using a combination of gray scale values and visual assessment of texture after thresholding to remove non-skeletal materials. Reconstructed scans are

reposited with their respective collections and requests for scans should be directed to those institutions as proper copyright holders of those data.

Landmarking

A two-dimensional geometric morphometric approach in R (R Core Team, 2020) was used to quantify shape (code found at github.com/ZacharySMorris/AR-SI-Croc-21-0331). A total of 17 fixed landmarks (type I or II *sensu* Bookstein, 1991) and two semi-landmark curves (figure 1, table S3) were captured with the StereoMorph package (Olsen & Westneat, 2015; Olsen & Haber, 2017) and analyzed with the RRPP and geomorph packages (Collyer & Adams, 2018, 2021; Adams et al., 2021). The fixed landmarks defined the overall shape of the skull, including the infratemporal fenestra, orbit, skull roof, jaw margin, and the pterygoid. Discrete landmarks (red dots in figure 1) were chosen to maximize both the amount of shape captured and the number of embryos to be included in the analysis. Several landmarks were positioned at points of sutural contact in adults (landmarks 2-4, 7, 9, 10, 15, & 16) in order to capture changes in skull architecture, however, young embryos often lack sutures that form later in ontogeny. To both account for and quantify these transformations, landmarks were defined as the anterior- or posterior-most extent of a key element (bolded in Table S3) across ontogeny and were positioned at the end of this bone when sutural contact was weak and at the point of contact when apparent. The first semi-landmark curve followed the profile of the face (green line in figure 1) from the suture between the postorbital and frontal on the posterodorsal edge of the orbit to the tip of the snout (anchored by landmarks 1 and 9). The second semi-landmark curve traversed the dorsolateral ridge of the skull table (blue line in figure 1) along the squamosal and postorbital (squamosal-postorbital bar; anchored by landmarks 6 and 8). In a small number of specimens (table S4) it was not possible to place landmarks on the pterygoid or the suture between the frontal and prefrontal (landmarks 10, 16, 17) due to damage or obstruction by other elements (e.g., lower jaw, palpebral), so their position was estimated based on the variance in the total dataset using the thin-plate spline method (*estimate.missing*). This method maintains the variance of the dataset and results in minimal error compared to the loss of data caused by excluding specimens. During Procrustes superimposition (*gpagen*), the semi-landmarks were downsampled to seven points per curve and allowed to slide to minimize the bending energy and account for the reduced degrees of freedom compared with the fixed landmarks (Rohlf, 1990; Bookstein, 1997; Zelditch et al., 2012). Downsampling to seven semi-landmarks (5 sliding + two fixed at discrete landmarks) ensured the shape of each curve was adequately captured while not outnumbering the discrete landmarks in combined analysis. To reconstruct the ontogenetic trajectories of the curvature of the skull table and dorsal face in greater detail, individual curve analyses were conducted by sampling each with 20 points and allowing them to slide between the two anchoring landmarks.

Quantifying shape and ontogenetic trajectories

The shape of the lateral skull was quantified in three ways: 1) complete lateral skull with all landmarks and semi-landmarks, 2) skull table semi-landmark curve, and 3) dorsal face semi-landmark curve. The three datasets were analyzed and visualized using principal components analysis (PCA; *gm.prcomp*). To assess whether there were significant differences in multivariate skull shape (i.e., Procrustes aligned coordinates) among ecomorphs, Procrustes ANOVA (P-ANOVA; *lm.rrpp*) with pairwise comparisons (*pairwise*) was performed among ecomorphs at each ontogenetic stage (as separate factors). To further explore whether the ontogeny of the lateral skull shape differed among ecomorphs, allometric trajectories were calculated and P-ANOVA was used to test the effect of size (log transformed centroid size as a covariate) and ecomorph (as a factor) on multivariate skull shape based on the interaction term (size:ecomorph). The common allometric component (CAC) for each morphospace was used to visualize ontogenetic trajectories (*plotAllometry*) and vector diagrams were used to visualize the changes in shape across ontogenetic trajectories and PC axes (*plotRefToTarget*).

When ontogenetic trajectories were visualized for all three datasets (but particularly the two curve-only analyses), there were noticeable differences in the association between shape and size among the smaller (embryonic) and larger (post-hatching) individuals in our sample. Therefore, linear regression with multiple change points (i.e. "broken-stick regression") was performed using the mcp package (Lindeløv, 2020). A null model with no breaks and a single slope was compared to alternative models with 1) a single break, 2) a single break for each species, and 3) a single break for each ecomorph. The model with the highest estimated log predictive density (ELPD) and lowest standard error (SE) was preferred and deemed a significantly better fit when comparisons to other models had an □ELPD/□SE ratio of greater than five. Subsequently, P-ANOVA was re-run on subsets of the data to test for differences among ecomorphs in the trajectories for embryonic development and post-hatching growth, separately, as the break point was always recovered near the largest embryonic specimens.

Results

Complete lateral skull morphospace

The complete lateral skull morphospace generated via PCA (figure 2a) shows that the first principal component (PC1) summarizes 79.9% of the variation and that the variance is highly correlated with size (Pearson correlation coefficient, PCC = 0.9176, table S5). The most dramatic variation observed across PC1 is in the length of the snout, slope of the frontal bone, relative size of the orbit and infratemporal fenestra, orientation and curvature of the skull table, and position of the jaw joint (figure 3a). The second PC explains 9% of the variance and shows changes in the degree of curvature of the skull table (highly curved to flat), but also additional variation in the position of the jaw joint (relative to the posterior edge of the skull), the size and rostro-caudal position of the pterygoid buttress, and the height of the snout.

Adults of all ecomorphs fall on the more positive end of PC1 with greater spread in PC2 scores. The majority of the negative PC1 region is exclusively occupied by embryonic specimens (red region in figure 2a), reflecting their much shorter faces with more inclined facial curves, larger orbits, and substantially more curved and depressed braincases. Only *G. gangeticus* and *T. schlegelii* embryos fall outside of this region (purple region in figure 2a), primarily due to their substantially longer faces and less steeply inclined curvature of the frontal in the orbital region. In contrast to post-hatching individuals, embryos showed substantially less variation along PC2.

At the mid-skeletal stage, embryos of different ecomorphs do not possess distinct skull shapes ($p = 0.108$, table S6), with the exception of *G. gangeticus* which clusters with the late-skeletal stage embryos of *T. schlegelii*. However, all other ontogenetic stages show significant differences in skull shape among ecomorphs ($p < 0.036$ after correction for multiple comparisons).

Dorsal face morphospace

The PCA of the dorsal face curve (2 fixed and 18 semi-landmarks; figure 2c,d) shows that variation is primarily distributed across the first three PCs (65.3%, 16.8%, and 10.8%). Along PC1 the major shape changes are in the orientation and length of the snout relative to the orbital region. While the snout remains similar in relative height across this axis, the snout is substantially downward pitched (anteroventrally angled) relative to the orbit at highly negative values, while at positive values the snout is horizontal as is typical for adult crocodylians (figure 3b). The negative PC1 region of morphospace is occupied by mostly embryonic individuals who possess a highly posteroventrally curved region in front of the orbit, followed by a less dramatic anterodorsally concave transition into the snout. At the extreme positive end of PC1, the profile of the orbit slopes more gradually and the major curvature of the snout encompasses an anterordorsally concave transition into the snout and a ventral turn at the tip of the snout.

The profile of the face in individuals with more positive PC2 values are generally flatter due to having taller rostral ends and a much more dramatic downward curvature at the tip of the snout, while those in the negative PC2 region of morphospace show a greater dorsal concavity in the middle of the snout and a more dorsally positioned rostral tip. The positive PC3 region of morphospace is also characterized by much flatter faces along the entire curve, while the negative region is much more dorsally concave in the middle with a more dramatic ventral slope at the tip of the snout. Across PC2 there is substantial overlap of ecomorphs, but slender and blunt adults were more distinct in their PC3 values.

Similar to the complete skull morphospace, ecomorphs were distinct in shape at all ontogenetic stages except for mid-skeletal period embryos ($p = 0.065$, table S7). Interestingly, the patterns of morphospace occupation are remarkably similar between the first two PCs of the complete skull morphospace and the first and third PCs of the dorsal face curve only morphospace (although embryonic *G. gangeticus* and *T. schlegelii* specimens do overlap with adult blunt forms).

Skull table morphospace

The PCA of the skull table curve (2 fixed and 18 semi-landmarks; figure 2b) shows that PC1 captures almost all the variance in the dataset (85.6%) and that this variation is strongly correlated with size (PCC = 0.7075, table S5). Along PC1 (figure 3c), the ridge on the dorsolateral edge of the skull table transforms from highly curved with an asymmetric sigmoidal shape (negative PC1) to nearly flat with a slightly higher posterior end (positive PC1). The second PC (6.5% of the variation) summarizes differences in the rostral-most points of the curve and whether they are more dorsally positioned (negative PC2) or ventrally positioned (positive PC2) relative to the rest of the skull table.

Similar to the total dataset, embryos occupy the negative PC1 region of morphospace, while larger individuals tend to have more positive PC1 values. The maximum PC1 score was less than half that of the complete skull morphospace, likely reflecting that the skull table can only become so flat and changes in skull shape are much more dramatic during embryonic development. Unlike the patterns observed for the complete skull or the dorsal face curve in isolation, there are no clear differences in skull table shape among ecomorphs at any ontogenetic stage except for the mid-skeletal stage embryos ($p = 0.012$, table S8). However, this result may be an artifact of greater sampling of the youngest embryos among moderate ecomorph species compared to the blunt and slender forms, as pairwise comparisons reveal only moderate embryos are distinct ($p < 0.008$).

Ontogeny of the complete lateral skull

When plotted in allometric space (figure 4a), the complete lateral skull dataset reveals a slight asymptotic trend with a faster rate of shape change among the embryonic specimens that levels out at larger sizes. There are substantial changes in the shape of the skull from the smallest embryos to the largest adults, with the majority occurring during embryonic development. The most significant changes across ontogeny are reorientation and elongation of the snout, decrease in relative size of the orbit and infratemporal fenestrae, posteroventral shift in the jaw joint and pterygoid buttress, and flattening of the curvature of the skull table. Ecomorphs do not differ substantially in their embryonic trends, with the lone *Gavialis* embryo as the only obvious outlier. Despite occupying a distinct region of morphospace alongside *Gavialis*, the *Tomistoma* embryos and hatchlings follow the same embryonic trajectory as other crocodylians. Slender-snouted forms achieve greater CAC values and are separated from blunt and moderate ecomorphs at larger sizes ($\log(CS) > 2$), while blunt and moderate forms overlap to a greater degree.

Comparisons of linear regression models that allow change points and variability among species or ecomorphs support the slightly asymptotic nature of these ontogenetic trajectories, as all models that include a single breakpoint are preferred over the null which does not allow changes in trajectory (table S9). The top two models allow species or ecomorphs to differ in their trajectory (slope and intercept) at larger sizes, but hold a common ontogenetic trajectory for small individuals

(log(CS) < 2.234 and 2.266). The pooled embryonic allometric trajectory has a substantial positive slope (mean slope = 0.214), while the pooled post-hatching trajectory is less steep but still positive (mean slope = 0.065). The slender ecomorph crocodylians follow a significantly flatter ontogenetic trajectory across all of ontogeny (p = 0.009), but moderate and blunt forms are not distinct from each other (table S10). The uniquely slender snouted embryos of *Gavialis gangeticus* and *T. schlegelii* possess a unique mean shape relative to all others (p = 0.033) which again causes a slightly flatter embryonic ontogeny among slender ecomorphs (table S10). No other pairwise differences were detected among embryos.

Ontogeny of the dorsal face

The ontogeny of the dorsal face curve is similar to the complete skull in terms of the amount of shape change observed during embryonic and post-hatching stages, although with less separation among ecomorphs at large size (figure 5). Model comparisons (table S9) prefer a single break point near the end of embryonic development (log(CS) ~ 1.896). Comparison of ecomorph specific allometric trends show no differences among embryonic specimens (table S11), but differences were recovered during total and post-hatching ontogeny as the slender ecomorph ontogeny was considerably flatter.

More dramatic changes in the curvature of the face are seen during the common embryonic development trajectory (figure 5), which includes a decrease in the curvature surrounding the orbit, a decrease in the angle of the snout relative to the orbit, and a deepening of the dorsal concavity in the boundary between the orbit and the snout. These changes in shape are also concurrent with a shift in orientation of the profile of the face from one with a substantial dorsoventral slope to one which is horizontally oriented. Although the slope of post-hatching ontogenetic trajectories for the dorsal face curve are flatter than for the complete lateral skull dataset, the ecomorph specific trajectories capture slight differences in the lengthening of the snout, posterior shifting of the slope from the orbit to the snout, and changes in the depth of the snout. The changes in shape captured by this curve, although removed from their orientation and size, are still coincident with important changes in the orientation of the face and the length of the snout.

Ontogeny of the skull table

The ontogeny of the skull table curve shows a remarkably different pattern from that observed in the complete lateral skull and dorsal face. Importantly, nearly all of the flattening of the skull table occurs embryonically and subsequent changes during post-hatching growth are relatively minor (figure 6). Among the smallest individuals there is a trend of increasing CAC values with increasing size (PCC = 0.628), but larger specimens (log(CS) > 2) show no association between size and shape (PCC = 0.095). There is also remarkable overlap of ecomorphs across ontogeny, without any hint of separation like that observed in the complete skull or dorsal face.

Model comparison found that a single break point (log(CS) ~ 2.26) near the size of the largest embryos (log(CS) = 1.92) with two separate linear models is a significantly better fit (table S9) than no breakpoint. Models which allow for different trajectories for each species or ecomorph do not perform better. To confirm these findings, additional P-ANOVA tests were performed on embryonic and post-hatching subsets, individually. Despite showing significant association between shape and size (p = 0.009), there are no ecomorph specific allometric trends during embryonic development (table S12). Comparison of post-hatching ontogenetic trajectories further reveals no differences in the allometric trends among ecomorphs (P = 0.585 , table S12). The slope of the pooled post-hatching allometric trajectory is nearly zero (mean slope = -0.0048), demonstrating that after the end of embryonic development essentially no further change in the curvature of the skull table occurs, despite increasing in size by two orders of magnitude. In contrast, while the embryonic skull only doubles in size, the shape of the skull table transforms from highly curved with a ventrally oriented

posterior end to the essentially flattened adult condition with only a slight ventral deflection at the posterior end (figure 6).

Discussion

Embryonic origin of the flattened crocodylian skull

The iconic flatness of the crocodylian skull arises from three key features: the platyrostral snout, the flat skull table, and the laterally flared jaw joint. The functional consequences of this skull conformation as compared to an ancestrally tall, oreinirostral archosaur skull have been previously explored (Busbey, 1995), including the influence on muscular anatomy (Holliday & Witmer, 2007), feeding mechanics (Rayfield & Milner, 2008), and hydrodynamic performance (McHenry et al., 2006). However, the developmental origins of the distinctive flatness of the crocodylian skull remain poorly understood outside of cursory mention in qualitative descriptions (e.g., Ferguson, 1985; Iordansky, 1973). Our study demonstrates that at the inception of cranial ossification, embryos possess a unique skull shape, neither platyrostral or oreinirostral, with an enlarged orbit, highly curved skull roof, and a short, steeply angled snout (figures 4-6). Critically, the complete lateral skull morphospace (figure 2) reveals that embryos of blunt, moderate, and slender ecomorphs share this unique embryonic shape, similar to the conserved embryonic region (CER) recovered for dorsal skull shape (Morris et al., 2019). Only *Gavialis* and *Tomistoma* embryos fell outside the CER in the lateral skull (purple region in figure 2) and dorsal skull morphospaces (Morris et al., 2019), due to their more elongated snouts. Similar embryonic patterns have been observed within other vertebrate clades (Sanger et al., 2013; Powder et al., 2015; Camacho et al., 2019) and across amniotes during earlier craniofacial morphogenesis (Young et al., 2014), indicating strong developmental conservation prior to ossification. However, the conservation of crocodylian lateral skull ontogeny extends beyond the CER to include the subsequent embryonic transformations in cranial anatomy.

From the CER embryos undergo several dramatic transformations prior to hatching: substantial elongation of the snout, decrease in relative size of the orbit and infratemporal fenestra, movement of the jaw joint posterior to the squamosal, posteroventral elongation of the pterygoid buttress, and reorientation of the profile of the face, skull table, and jaw margin to become nearly horizontal (figures 4-6). Across all three datasets analyzed here, the embryonic ontogenetic trajectories were similar among all ecomorphs (table S10-12). The extremely slender-snouted *Gavialis* and *Tomistoma* embryos may follow a different pattern, as they are furthest from the common embryonic trajectories, but low sample size in these species results in equivocal results. These shared ontogenies extend until a conspicuous break point near the upper size range of embryos (figures 4-6, table S9), at which point the rate of shape change decreases considerably. In fact, there is essentially no change in the curvature of the skull table across post-hatching ontogeny and the adult condition is achieved by or just after hatching in our dataset (figure 6). Differences are detected among ecomorphs in the post-hatching ontogeny of the complete lateral skull (figure 4) and the snout profile (figure 5), reflecting differences in snout proportions among ecomorphs. No such shift between embryonic and post-hatching ontogeny was observed for dorsal skull shape (Morris et al., 2019), indicating the evolution of lateral skull ontogeny is not driven by the same heterochronic processes as found for dorsal snout proportions. Nevertheless, our data show that for most crocodylian species, the majority of change in lateral skull shape occurs prior to hatching and occurs along a common ontogenetic trajectory.

Skeletal rotation during development generates cranial flatness

Anatomical investigation of the embryos in our dataset reveals that the flatness of the crocodylian lateral skull is not achieved by active ‘compression’ or via negative allometry relative to the rest of the skull during development. Rather, horizontality is primarily achieved by rotation of skeletal elements of the snout and skull table relative to the orbit and basicranium.

The curvature of dorsal face is initially dominated by the orbit and the major skeletal elements of the snout (maxillae, nasal, and premaxillae) are comparatively dorsoventrally compressed. However, these elements are oriented at a steep anteroventral angle relative to the posterior skull among the youngest embryos (figure 5). Across embryonic development these elements progressively elongate and rotate together such that the jaw margin becomes horizontal prior to hatching. During initial ossification, the basicranial axis follows a highly curved path from a noticeably bent neck to a snout and jaw margin that are offset from the posterior skull (Ferguson, 1985; *pers. obv.*). The rotation of an already compressed snout is, thus, the final step in the flattening of the basicranial axis and generation of the platyrostral snout.

The squamosal-postorbital bar is only partially ossified among the youngest embryos and the dorsolateral edge of the skull table possesses an asymmetric sigmoidal shape as the posterior end overlies the relatively large brain and highly domed head. The initial ossification of the squamosal occurs in a relatively more ventral position and the external surface is primarily laterally oriented (figure 7). Across embryonic development the squamosal expands, rotates, and flattens, such that the dorsal edge becomes medially oriented and forms the lateral margin of the supratemporal fenestra and the ornamented surface shifts to the dorsal side of the skull table (figure 7). This rotation around the rostrocaudal axis is crucial to the formation of the crocodylian external ear, as it creates both the recess for the tympanic membrane and the attachment for the dorsal earflap that keeps the tympanic membrane dry when submerged (Shute & Bellairs, 1955; Iordansky, 1973).

The embryonic reorientations of these bones are fundamental to the flatness of the crocodylian skull and are conserved across species and ecomorphs (figures 4-6), with even *Gavialis* embryos possessing a more laterally oriented squamosal at the youngest stages. Across these same stages of development, the neck and brain both reorient to become more horizontal (Lessner & Holliday, 2020), confirming that the reorientation of the snout, skull table, and mandible are coordinated with a reorientation of the entire head. Although the flaring of the quadrate is poorly captured in our dataset, the jaw joint appears to move posteroventrally across ontogeny and this also likely involves important changes in the orientation of the quadrate (figure 4). Therefore, it is clear that rotation of partially ossified bones is a key mechanism underlying the development of cranial flatness. This further emphasizes how embryonic development of lateral skull shape, both before and after the initiation of ossification, has been remarkably conserved across Crocodylia.

Factors underlying conservation of embryonic development

The contrast between the dramatic transformations during embryonic development and the limited shape change after hatching is striking and suggests strongly that distinct factors may drive the evolution of embryonic and post-hatching ontogenetic patterns. One possible explanation for the breakpoint in development is strong selective pressure on hatchlings, as hatchling crocodylians likely experience greater mortality than other age classes (Somaweera et al., 2013). Although the specific selective pressures on hatchling snout profile have not been investigated, biomechanical modeling suggests that platyrostral snouts encounter less drag during aquatic feeding and locomotion (McHenry et al., 2006) and hydrodynamic performance likely played a key role in the evolution of crocodylian snout shape (Cleuren and Vree, 2000; Pierce et al., 2008). The proper alignment of the jaw margin and orientation of the pterygoid buttress are also critical for effective generation of bite forces (Gignac and Erickson, 2016; Sellers et al., 2017). Additionally, the rotation of the skull table may be important for proper alignment between the external ear and paratympanic sinuses, which together create a pressure difference receiver that improves sound localization at the water-air boundary (Bierman et al., 2014; Bierman & Carr, 2015). This specialized ear is likely critical for both localization of prey and communication with parents, which begins prior to hatching (Somaweera et al., 2013). Newly hatched crocodylians quickly enter aquatic environments and must actively navigate their environment for survival (Grigg & Kishner, 2015), which makes it likely that these factors act as important selective pressures on hatchling skull shape.

Although selection on hatchling performance may explain the shift in developmental rate, in isolation it is unlikely to generate the conservation of embryonic developmental patterns observed across crocodylians. The common embryonic trajectory from the CER to similar hatchling skull shapes suggest that developmental constraint may also play an important role. Constraint has been implicated in the remarkable conservation of developmental patterns across major clades during organogenesis (Duboule, 1994; Irie and Kuratani, 2011; Abzhanov, 2013), craniofacial morphogenesis (Young et al., 2014), and even during later skeletal development within less inclusive vertebrate clades (Sanger et al., 2013; Powder et al., 2015; Camacho et al., 2019; Morris et al., 2019). Stabilizing selection due to pleiotropic effects from modifications among tightly integrated developmental modules (genetic and anatomical) has been suggested to both limit variation at 'phylotypic stages' and bias the evolution of later developmental patterns (Zalts and Yanai, 2017; Galis et al., 2018). Therefore, the crocodylian cranial CER and conserved ontogenetic transformations likely reflect constraints on embryonic development from earlier genetic patterning and/or direct physical interactions with other tissues. This may be particularly true for the skull table and the brain, given the high covariation between the brain and braincase (Fabbri et al., 2017). When considered together, it appears highly probable that a combination of developmental constraint and selective pressure on skull shape at hatching have resulted in the canalization of lateral skull ontogeny and the rate shift near the end of embryonic development.

Evolutionary origins of cranial flatness

The conservation of developmental patterns of the lateral skull across ecomorphs implies that these aspects of cranial ontogeny are likely ancestral for crown Crocodylia. However, the major components that contribute to the overall flatness of the crocodylian skull first appear much earlier in the fossil record. The platyrostral snout can be traced back to at least the Middle Jurassic in early neosuchians and is broadly retained in both goniopholidids and eusuchians (Rayfield & Milner, 2008; Pol et al., 2013), while there is a clear conservation of an expanded skull table and external ear anatomy since at least the divergence of Crocodyliformes in the Late Triassic (Pol et al., 2013; Montefeltro et al., 2016). Although the fossil record reveals the 're-evolution' of deep-snouted forms among notosuchians and pristichampids and remarkably open skull roofs among thalattosuchians, these are clearly restricted to specific clades and actually highlight the remarkable stability of key features such as the rotated squamosal and platyrostral snouts across 225 and 170 million years of evolution, respectively. This begs the question, whether the ontogeny of these distinct components themselves first evolved among stem crocodylians and has been retained among extant species?

Despite the lack of fossilized developmental series of stem crocodylians, the evidence for developmental constraints on embryonic skull shape in crocodylians and even earlier stages of morphogenesis across vertebrates hint that the shape of the lateral skull during initial ossification evolved outside of crown Crocodylia. Amniotes also share conserved cellular mechanisms of facial outgrowth (Morris & Abzhanov, 2021) and the molecular pathways which direct skull roof formation appear to be conserved in at least reptiles and birds (Abzhanov et al., 2007; Tokita et al., 2013). Although the proximal mechanisms for skull table flattening remain unclear, physical interactions and signaling from the developing brain likely play important roles given the high covariation between the brain and braincase (Fabbri et al., 2017). The conservation of key aspects of the flattened skull in adults across crocodyliform evolution (e.g., dorsally rotated squamosal, flared quadrates, low profile snouts) and the constrained processes and patterns of embryonic development suggest it is plausible that similar ontogenetic transformations may have facilitated the evolution of the flattened skull. Critically, the rotations of key skeletal elements of the skull table and snout are likely fundamentally necessary for the generation of a flattened skull from the constrained embryonic origin found among crocodylians and other amniotes (Young et al., 2014). While it is difficult to determine precisely when modern developmental patterns first evolved, and somewhat speculative to even attempt without fossilized evidence, these findings suggest that key features of the

crocodylian cranial developmental program may have evolved as early as 225 and 170 million years ago, respectively.

Conclusions

Our analysis of crocodylian lateral skull ontogeny has revealed a remarkably conserved pattern of skeletal transformations from a shared embryonic skull shape. The similarities to other stages of developmental conservation across vertebrates implies that a significant constraint exists on the shape of the skull during initial ossification and a conservation of earlier molecular and cellular processes. However, unlike the evolution of dorsal snout proportions in crocodylians, we do not find evidence of divergence or heterochronic modifications in embryonic developmental patterns among ecomorphs. Except for potential differences in pre-skeletal developmental processes in *Gavialis* and *Tomistoma*, developmental constraint and/or selection on hatchling anatomy appear to have resulted in substantial conservation of embryonic development of lateral skull shape in Crocodylia. Although the proximal developmental mechanisms generating the initial shape of the skull and subsequent craniofacial ontogeny remain to be investigated, it is clear that the rotation of snout and skull roof elements are critical anatomical transformations in generating the iconic flatness of the crocodylian skull. The ancient origin of platyrostral snouts and flat skull tables suggest that these developmental patterns may predate the divergence of extant crocodylians and could indicate the conservation of embryonic development for upwards of 225 million years.

Acknowledgments

For assistance with collections access we thank: J. Cundiff and J. Rosado (Museum of Comparative Zoology); M. Brown and J. Sagebiel (Texas Memorial Museum, Vertebrate Paleontology Laboratory); P. Holroyd (University of California Museum of Paleontology); D. Brinkman and M. Fox (Yale Peabody Museum of Natural History); S. Miller (Campbell Geology Museum, Clemson University); A. Millhouse (National Museum of Natural History); and P. Campbell (British Museum of Natural History). The St. Augustine Alligator Farm and Rockefeller Wildlife Refuge both donated embryos which were included in this analysis and we are grateful for the support of their staff, including S. Isberg. M. Kerr and M. Whitlock scanned several embryonic specimens and N. Vitek photographed specimens used in this analysis. We also thank editors Emma Schachner and Casey Holliday for the invitation to submit for this special volume.

Literature Cited

Abzhanov A. 2013. von Baer's law for the ages: lost and found principles of developmental evolution. *Trends Genet* 29:712–722.

Abzhanov A, Rodda SJ, McMahon AP, and Tabin CJ. 2007. Regulation of skeletogenic differentiation in cranial dermal bone. *Development* 134:3133–3144.

Adams DC, Collyer ML, Kaliontzopoulou A, and Balken E. 2021. Geomorph: Software for geometric morphometric analyses. R package version 3.3.2. https://cran.r-project.org/package=geomorph.

Benton M, Donoghue P, Vinther J, Asher R, Friedman M, and Near T. 2015. Constraints on the timescale of animal evolutionary history. *Palaeontol Electron* 18.1.1FC:1–106.

Bierman HS, and Carr CE. 2015. Sound localization in the alligator. *Hearing Res* 329:11–20.

Bierman HS, Thornton JL, Jones HG, Koka K, Young BA, Brandt C, Christensen-Dalsgaard J, Carr CE, and Tollin DJ. 2014. Biophysics of directional hearing in the American alligator (*Alligator mississippiensis*). *J Exp Biol* 217:1094–1107.

Bookstein FL. 1997. Landmark methods for forms without landmarks: morphometrics of group differences in outline shape. *Med Image Anal* 1:225–243.

Brochu CA. 2001. Crocodylian snouts in space and time: phylogenetic approaches toward adaptive radiation. *Am Zool* 41:564–585.

Busbey AB. 1995. The structural consequences of skull flattening in crocodilians. In: Thomason, JJ, editor. *Functional morphology in vertebrate paleontology.* Cambridge University Press. p 173–192.

Camacho J, Heyde A, Bhullar B-AS, Haelewaters D, Simmons NB, and Abzhanov A. 2019. Peramorphosis, an evolutionary developmental mechanism in neotropical bat skull diversity. *Dev Dyn* 1:1–15.

Camacho J, Moon R, Smith SK, Lin JD, Randolph C, Rasweiler JJ, Behringer RR, and Abzhanov A. 2020. Differential cellular proliferation underlies heterochronic generation of cranial diversity in phyllostomid bats. *EvoDevo* 11:1–17.

Cleuren J and de Vree F. 2000. Feeding in crocodylians. In Schwenk K, editor. *Feeding*. Academic Press. ch. 10, p. 337–358

Collyer ML and Adams DC. 2018. RRPP: An R package for fitting linear models to high-dimensional data using residual randomization. *Methods Ecol Evol* 9: 1772-1779.

Collyer ML and Adams DC. 2021. RRPP: Linear Model Evaluation with Randomized Residuals in a Permutation Procedure. https://cran.r-project.org/web/packages/RRPP

Drumheller SK, Darlington J, and Vliet KA. 2019. Surveying death roll behavior across Crocodylia. *Ethol Ecol Evol* 31:1–19.

Drumheller SK and Wilberg EW. 2020. A synthetic approach for assessing the interplay of form and function in the crocodyliform snout. *Zool J Linn Soc*188:507–521.

Duboule D. 1994. Temporal colinearity and the phylotypic progression: a basis for the stability of a vertebrate Bauplan and the evolution of morphologies through heterochrony. *Development* Supplement:135–142.

Erickson GM, Gignac PM, Steppan SJ, Lappin AK, Vliet KA, Brueggen JD, Inouye BD, Kledzik D, and Webb GJW. 2012. Insights into the Ecology and Evolutionary Success of Crocodilians Revealed through Bite-Force and Tooth-Pressure Experimentation. *PLoS One* 7:e31781-12.

Fabbri M, Koch NM, Pritchard AC, Hanson M, Hoffman E, Bever GS, Balanoff AM, Morris ZS, Field DJ, Camacho J, Rowe TB, Norell MA, Smith RM, Abzhanov A, and Bhullar B-AS. 2017. The skull roof tracks the brain during the evolution and development of reptiles including birds. *Nat Ecol Evol* 1:1543–1550.

Ferguson MWJ. 1985. Reproductive biology and embryology of the crocodilians. In Gans C, Billett F, and Maderson PFA, editors. *Biology of the Reptilia*. John Wiley & Sons, New York, vol. 14 (Development A), ch. 5, p. 329–493

Gardiner DM, Torok MA, Mullen LM, and Bryant SV. 1998. Evolution of vertebrate limbs: robust morphology and flexible development. *Am Zool* 38:659–671.

Gignac PM and Erickson GM. 2016. Ontogenetic bite-force modeling of *Alligator mississippiensis*: implications for dietary transitions in a large-bodied vertebrate and the evolution of crocodylian feeding. *J Zoo* 299:229–238.

Gow CE. 2000. The Skull of *Protosuchus haughtoni*, an Early Jurassic Crocodyliform from Southern Africa. *J Vertebr Paleontol* 20:49–56.

Grigg G and Kershner D. 2015. Locomotion, Buoyancy and Travel. In *Biology and evoution of crocodylians*. Comstock Publishing Associates. Ch. 4, p. 133-171.

Holliday CM and Witmer LM. 2007. Archosaur adductor chamber evolution: Integration of musculoskeletal and topological criteria in jaw muscle homology. *J Morphol* 268:457–484.

Iordansky NN. 1973. The skull of the Crocodilia. In Gans C and Parsons TP, editors. *Biology of the Reptilia*. Academic Press, New York, vol. 4 (Morphology D), ch. 3, p. 201–262.

Irie N and Kuratani S. 2011. Comparative transcriptome analysis reveals vertebrate phylotypic period during organogenesis. *Nat Commun* 2:1–6.

Klein-Nulend J, Bacabac R, and Bakker A. 2012. Mechanical loading and how it affects bone cells: The role of the osteocyte cytoskeleton in maintaining our skeleton. *European Cells Mater* 24:278–291.

Langston, Jr. W. 1973. The Crocodilian Skull in Historical Perspective. In Gans C and Parsons TP, editors. *Biology of the Reptilia*. Academic Press, New York, vol. 4 (Morphology D), ch. 4, p. 263–284.

Lessner EJ and Holliday CM. 2020. A 3D ontogenetic atlas of *Alligator mississippiensis* cranial nerves and their significance for comparative neurology of reptiles. *Anat Rec* doi: 10.1002/ar.24550.

Lindeløv JK. 2020. mcp: An R package for regression with multiple change points. doi: 10.31219/osf.io/fzqxv

Ludwig MZ, Bergman C, Patel NH, and Kreitman M. 2000. Evidence for stabilizing selection in a eukaryotic enhancer element. *Nature* 403:564–567.

McHenry CR, Clausen PD, Daniel WJT, Meers MB, and Pendharkar A. 2006. Biomechanics of the rostrum in crocodilians: A comparative analysis using finite-element modeling. *Anat Rec* 288A:827–849.

Montefeltro FC, Andrade DV, and Larsson HCE. 2016. The evolution of the meatal chamber in crocodyliforms. *J Anat* 228:838–863.

Morris ZS and Abzhanov A. 2021. Heading for higher ground: Developmental origins and evolutionary diversification of the amniote face. *Curr Top Dev Biol* 141:241–277.

Morris ZS, Vliet KA, Abzhanov A, and Pierce SE. 2019. Heterochronic shifts and conserved embryonic shape underlie crocodylian craniofacial disparity and convergence. *Proc R Soc B* 286:20182389.

Narváez I, Brochu CA, Escaso F, Pérez-García A, and Ortega F. 2016. New Spanish Late Cretaceous eusuchian reveals the synchronic and sympatric presence of two allodaposuchids. *Cretac Res* 65:112–125.

Olsen AM and Haber A. 2017. StereoMorph: Stereo Camera Calibration and Reconstruction. Version 1.6.1. https://CRAN.R-project.org/package=StereoMorph.

Olsen AM and Westneat MW. 2015. StereoMorph: an R package for the collection of 3D landmarks and curves using a stereocamera set-up. Methods in Ecology and Evolution 6:351-356. DOI: 10.1111/2041-210X.12326.

Pierce SE, Angielczyk KD, and Rayfield EJ. 2009. Morphospace occupation in thalattosuchian crocodylomorphs: skull shape variation, species delineation and temporal patterns. *Palaeontology* 52:1057–1097.

Pierce SE, Angielczyk KD, and Rayfield EJ. 2008. Patterns of morphospace occupation and mechanical performance in extant crocodilian skulls: A combined geometric morphometric and finite element modeling approach. *J Morphol* 269:840–864.

Pol D, Rauhut OWM, Lecuona A, Leardi JM, Xu X, and Clark JM. 2013. A new fossil from the Jurassic of Patagonia reveals the early basicranial evolution and the origins of Crocodyliformes. *Biol Rev* 88:862–872.

Powder KE, Milch K, Asselin G, and Albertson RC. 2015. Constraint and diversification of developmental trajectories in cichlid facial morphologies. *EvoDevo* 6:1–14.

R Core Team (2020). R: A language and environment for statistical computing. R Foundation for Statistical Computing, Vienna, Austria. URL https://www.R-project.org/.

Rayfield EJ and Milner AC. 2008. Establishing a framework for archosaur cranial mechanics. *Paleobiology* 34:494–515.

Richardson MK. 2012. A Phylotypic Stage for All Animals? *Dev Cell* 22:903–904.

Rohlf FJ. 1990. Morphometrics. *Annu Rev Ecol Evol Syst* 21:299–316.

Sanger TJ, Seav SM, Tokita M, Langerhans RB, Ross LM, Losos JB, and Abzhanov A. 2014. The oestrogen pathway underlies the evolution of exaggerated male cranial shapes in Anolis lizards. *Proc R Soc B* 281:20140329.

Sanger TJ, Sherratt E, McGlothlin JW, Brodie ED, Losos JB, and Abzhanov A. 2013. Convergent evolution of sexual dimorphism in skull shape using distinct developmental strategies. *Evolution* 67:2180–2193.

Sellers KC, Middleton KM, Davis JL, and Holliday CM. 2017. Ontogeny of bite force in a validated biomechanical model of the American alligator. *J Exp Biol* 220:2036–2046.

Shute CCD and Bellairs Ad'A. 1955. The external ear in Crocodilia. *P Zool Soc Lond* 124:741–749.

Somaweera R, Brien M, and Shine R. 2013. The Role of Predation in Shaping Crocodilian Natural History. *Herpetol Monogr* 27:23–51.

Stocker MR and Butler RJ. 2013. Phytosauria. In Nesbitt SJ, Desojo JB, and Irmis RB editors. *Anatomy, phylogeny and palaeobiology of early archosaurs and their kin.* Geological Society, London, Special Publications, vol. 379, pp. 91–117.

Tokita M, Chaeychomsri W, and Siruntawineti J. 2013. Skeletal gene expression in the temporal region of the reptilian embryos: implications for the evolution of reptilian skull morphology. *Springerplus* 2:336.

Wilberg EW. 2017. Investigating patterns of crocodyliform cranial disparity through the Mesozoic and Cenozoic. *Zool J Linn Soc* 181:189–208.

Wilberg EW, Turner AH, and Brochu CA. 2019. Evolutionary structure and timing of major habitat shifts in Crocodylomorpha. *Sci Rep* 9:1–10.

FIGURE LEGEND

Figure 1. Landmarking strategy. 17 Fixed landmarks (red dots) and two semi-landmark curves (skull table - blue curve, dorsal face - green curve) were digitized to quantify skull shape in lateral view of embryonic and post hatching crocodylians. Scale bars are one centimeter.

Figure 2. Morphospaces of crocodylian lateral skull ontogeny generated based on the complete lateral skull dataset (A), the skull table semi-landmark curve only (B), and the face profile semi-landmark curve only (C - PCs 1 & 2, D - PCs 1 & 3). The conserved embryonic region (CER - red polygon) in the complete skull analysis includes embryos of all ecomorphs except Gavialis gangeticus and Tomistoma schlegelii (purple region). Symbols are scaled to the size class of each developmental stage.

Figure 3. Vector diagrams depicting the changes in landmark position from the consensus (mean) shape to the extreme negative (minimum) and extreme positive (maximum) value for the first two principal components of the complete lateral skull morphospace (top), the face profile morphospace (middle), and the skull table morphospace (bottom).

Figure 4. Ontogeny of complete lateral skull shape. Specimen are plotted in an allometric space (left) to show the ontogeny of shape (common allometric component) change relative to centroid size (log transformed) for the common embryonic trajectory (red) and post-hatching trajectories for slender (blue), moderate (green), and blunt (yellow) ecomorphs. Silhouettes of specimens representing the start and end of each ontogenetic trajectory and the vector diagram depicting the changes in landmark position between these specimens visualize the changes in skull shape (right). The 95% confidence interval around ontogenetic trajectories are shown as shaded polygons.

Figure 5. Ontogeny of the platyrostral face. Specimen are plotted in an allometric space to show the ontogeny of shape (common allometric component) change relative to centroid size (log transformed) for the common embryonic trajectory (red) and post-hatching trajectories for slender (blue), moderate (green), and blunt (yellow) ecomorphs. Silhouettes of specimens representing the start and end of each ontogenetic trajectory and the vector diagram depicting the changes in landmark position between these specimens visualize the changes in curvature of the profile of the face. The 95% confidence interval around ontogenetic trajectories are shown as shaded polygons.

Figure 6. Ontogeny of the skull table. Specimen are plotted in an allometric space to show the ontogeny of shape (common allometric component) change relative to centroid size (log transformed) for the common embryonic (red) and post-hatching (gray) trajectories. Silhouettes of specimens representing the start and end of each ontogenetic trajectory and the vector diagram depicting the changes in landmark position between these specimens visualize the changes in skull table shape. The 95% confidence interval around ontogenetic trajectories are shown as shaded polygons.

Figure 7. Anatomical changes to the squamosal-postorbital bar across ontogeny in dorsal, lateral, and coronal transect views. The squamosal undergoes substantial reorientation - the dorsal (blue lines and arrows) and ventral (orange lines and arrows) edges at Ferguson stage 21 (FS 21) rotate across ontogeny and correspond to the medial and lateroventral edges in the adult. The position of the coronal section is represented by the red line in lateral view. Anatomical abbreviations: exoccipital (eo), infratemporal fenestra (itf), parietal (pa), postorbital (po), prootic (pro), quadrate (q), quadratojugal (qj), squamosal (sq), supratemporal fenestra (stf). Scale bar measures 1mm.

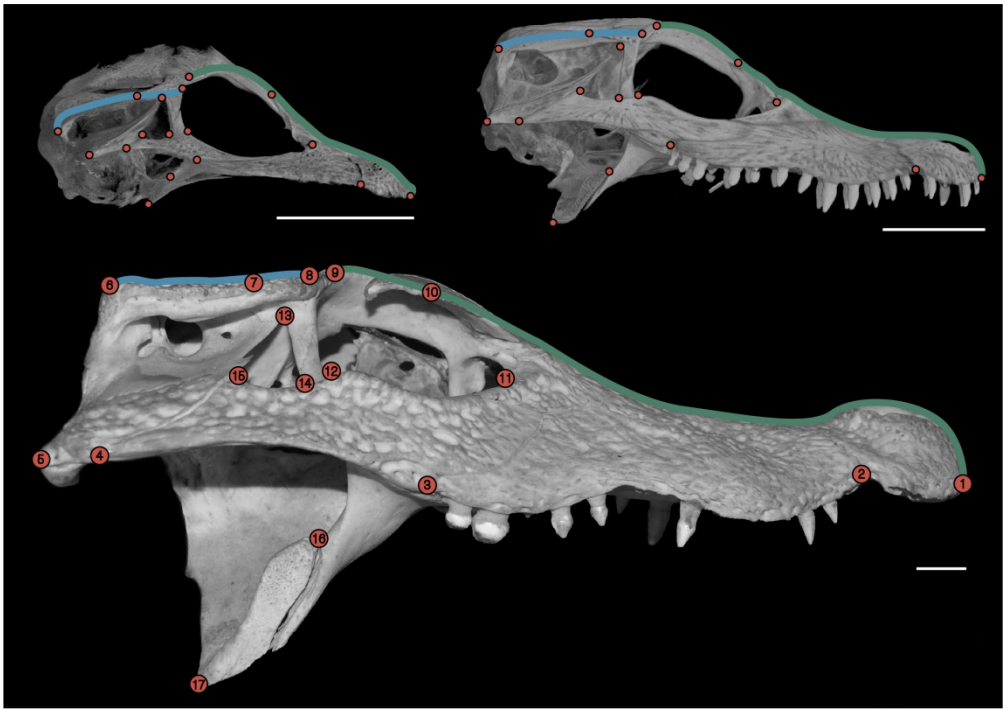

Figure 1. Landmarking strategy. 17 Fixed landmarks (red dots) and two semi-landmark curves (skull table - blue curve, dorsal face - green curve) were digitized to quantify skull shape in lateral view of embryonic and post hatching crocodylians. Scale bars are one centimeter.

254x179mm (300 x 300 DPI)

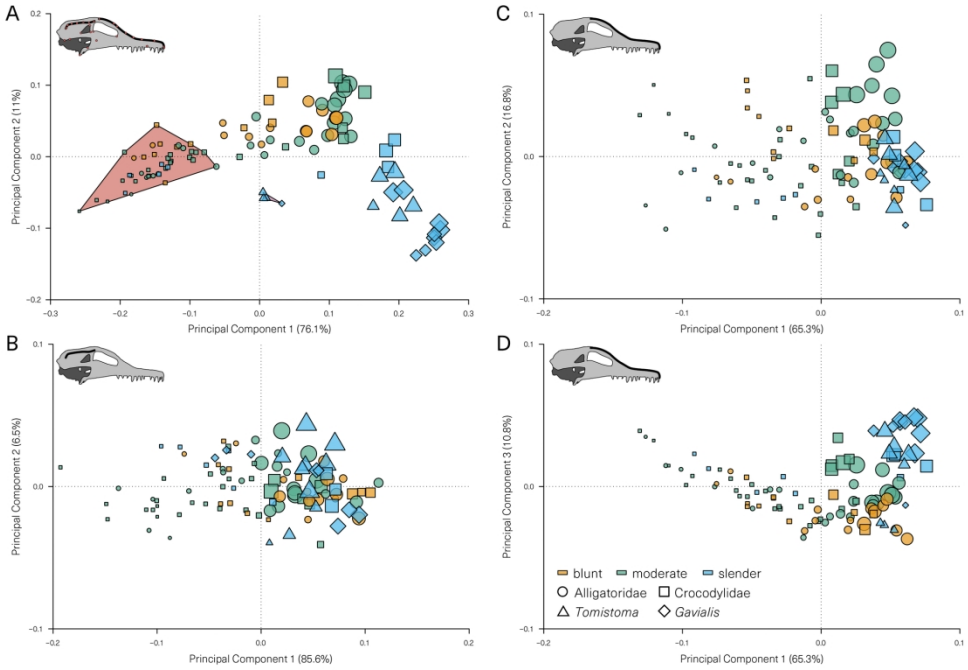

Figure 2. Morphospaces of crocodylian lateral skull ontogeny generated based on the complete lateral skull dataset (A), the skull table semi-landmark curve only (B), and the face profile semi-landmark curve only (C - PCs 1 & 2, D - PCs 1 & 3). The conserved embryonic region (CER - red polygon) in the complete skull analysis includes embryos of all ecomorphs except *Gavialis gangeticus* and *Tomistoma schlegelii* (purple region). Symbols are scaled to the size class of each developmental stage.

95x65mm (600 x 600 DPI)

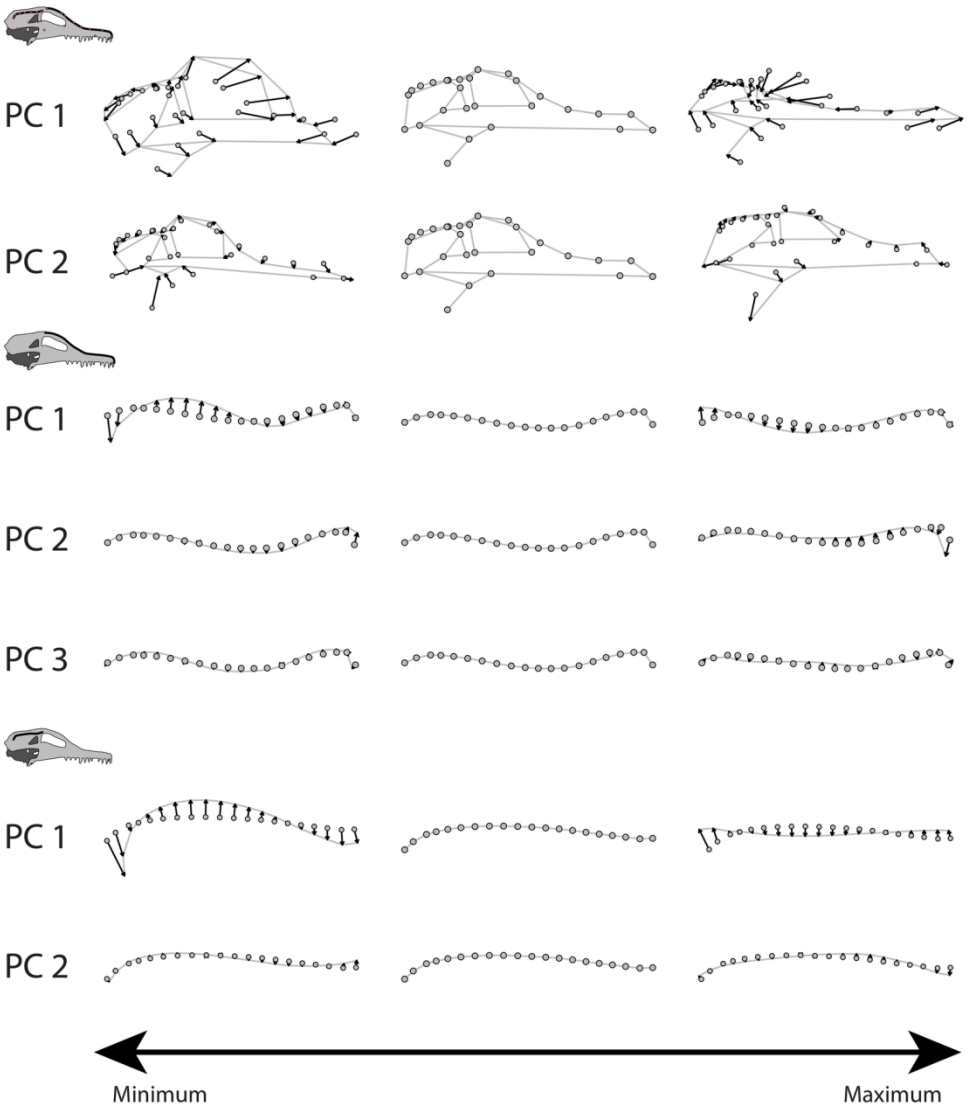

Figure 3. Vector diagrams depicting the changes in landmark position from the consensus (mean) shape to the extreme negative (minimum) and extreme positive (maximum) value for the first two principal components of the complete lateral skull morphospace (top), the face profile morphospace (middle), and the skull table morphospace (bottom).

74x82mm (600 x 600 DPI)

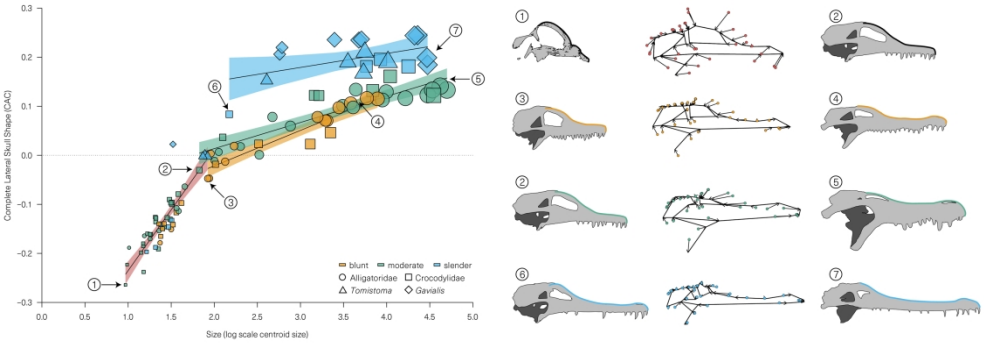

Figure 4. Ontogeny of complete lateral skull shape. Specimen are plotted in an allometric space (left) to show the ontogeny of shape (common allometric component) change relative to centroid size (log transformed) for the common embryonic trajectory (red) and post-hatching trajectories for slender (blue), moderate (green), and blunt (yellow) ecomorphs. Silhouettes of specimens representing the start and end of each ontogenetic trajectory and the vector diagram depicting the changes in landmark position between these specimens visualize the changes in skull shape (right). The 95% confidence interval around ontogenetic trajectories are shown as shaded polygons.

131x47mm (600 x 600 DPI)

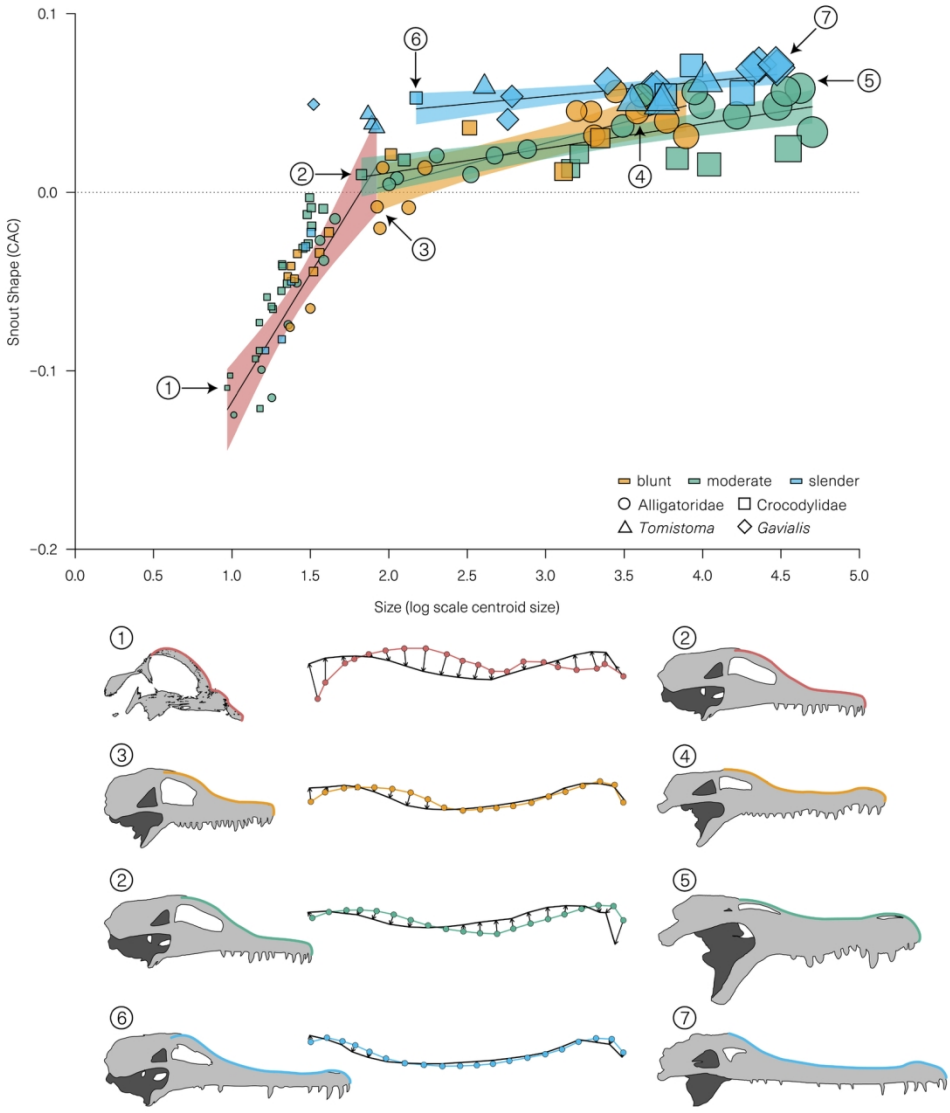

Figure 5. Ontogeny of the platyrostral face. Specimen are plotted in an allometric space to show the ontogeny of shape (common allometric component) change relative to centroid size (log transformed) for the common embryonic trajectory (red) and post-hatching trajectories for slender (blue), moderate (green), and blunt (yellow) ecomorphs. Silhouettes of specimens representing the start and end of each ontogenetic trajectory and the vector diagram depicting the changes in landmark position between these specimens visualize the changes in curvature of the profile of the face. The 95% confidence interval around ontogenetic trajectories are shown as shaded polygons.

73x86mm (600 x 600 DPI)

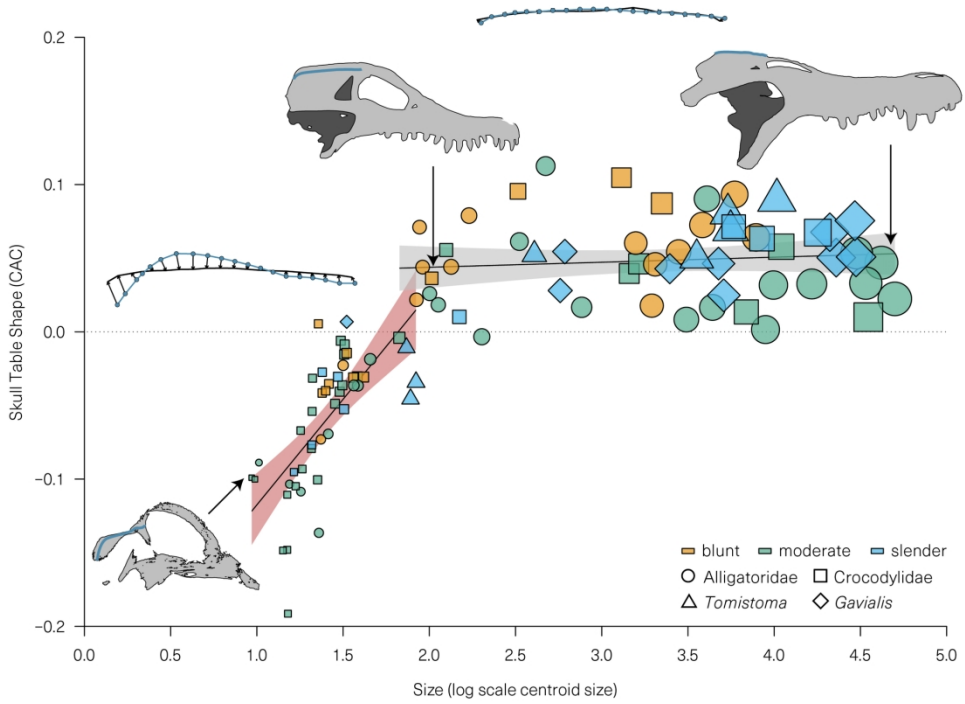

Figure 6. Ontogeny of the skull table. Specimen are plotted in an allometric space to show the ontogeny of shape (common allometric component) change relative to centroid size (log transformed) for the common embryonic (red) and post-hatching (gray) trajectories. Silhouettes of specimens representing the start and end of each ontogenetic trajectory and the vector diagram depicting the changes in landmark position between these specimens visualize the changes in skull table shape. The 95% confidence interval around ontogenetic trajectories are shown as shaded polygons.

90x68mm (600 x 600 DPI)

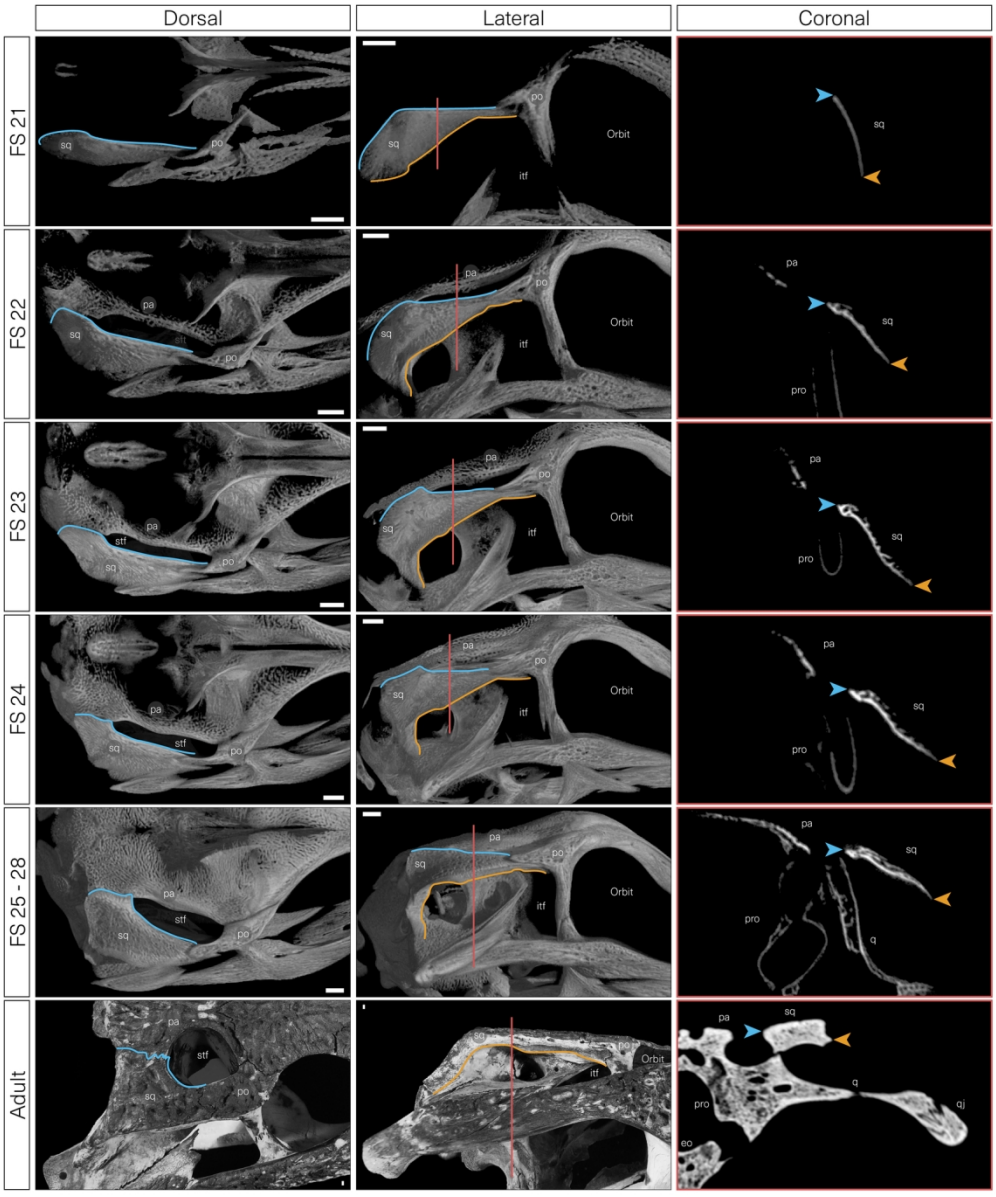

Figure 7. Anatomical changes to the squamosal-postorbital bar across ontogeny in dorsal, lateral, and coronal transect views. The squamosal undergoes substantial reorientation - the dorsal (blue lines and arrows) and ventral (orange lines and arrows) edges at Ferguson stage 21 (FS 21) rotate across ontogeny and correspond to the medial and lateroventral edges in the adult. The position of the coronal section is represented by the red line in lateral view. Anatomical abbreviations: exoccipital (eo), infratemporal fenestra (itf), parietal (pa), postorbital (po), prootic (pro), quadrate (q), quadratojugal (qj), squamosal (sq), supratemporal fenestra (stf). Scale bar measures 1mm.

145x173mm (300 x 300 DPI)

Table S1. Specimen list

Species	Specimen ID	Age
Alligator mississippiensis	ZAM E32 (Series 1)	Mid-Stage Embryo
Alligator mississippiensis	ZAM E37 (Series 1)	Mid-Stage Embryo
Alligator mississippiensis	ZAM E42 (Series 2)	Mid-Stage Embryo
Alligator mississippiensis	ZAM E46 (Series 1)	Mid-Stage Embryo
Alligator mississippiensis	ZAM E50 (Series 2)	Late-Stage Embryo
Alligator mississippiensis	ZAM E70 (Series 1)	Late-Stage Embryo
Alligator mississippiensis	MCZ 161018	Juvenile
Alligator mississippiensis	MCZ 61221	Juvenile
Alligator mississippiensis	TMM-M-253	Juvenile
Alligator mississippiensis	TMM-M-6707	Juvenile
Alligator mississippiensis	TMM-M-8664	Juvenile
Alligator mississippiensis	MCZ 81457	Subadult
Alligator mississippiensis	TMM-M-7846	Subadult
Alligator mississippiensis	TMM-M-983	Subadult
Alligator mississippiensis	MCZ 33949	Adult
Alligator mississippiensis	MCZ 43005	Adult
Alligator mississippiensis	TMM-M-4864	Adult
Alligator mississippiensis	TMM-M-67	Adult
Alligator mississippiensis	TMM-M-7388	Adult
Caiman crocodilus	BMNH 1898_10_11_2	Mid-Stage Embryo
Caiman crocodilus	UF 184575	Late-Stage Embryo
Caiman crocodilus	UF 184576	Hatchling
Caiman crocodilus	MCZ 32233	Juvenile
Caiman crocodilus	UCMP 138038	Juvenile
Caiman crocodilus	UCMP 123096	Juvenile
Caiman crocodilus	UCMP 123097	Juvenile
Caiman crocodilus	MCZ 5031	Subadult
Caiman crocodilus	MCZ R-194856	Subadult
Caiman crocodilus	MCZ 38661	Subadult
Caiman crocodilus	UCMP 123095	Subadult
Caiman crocodilus	UCMP 42843	Subadult
Caiman crocodilus	MCZ 3557	Adult
Caiman crocodilus	MCZ 46632	Adult
Crocodylus moreletii	CSUC 1633a	Mid-Stage Embryo
Crocodylus moreletii	CSUC 1633b	Mid-Stage Embryo
Crocodylus moreletii	CSUC 1633c	Mid-Stage Embryo
Crocodylus moreletii	CSUC 1633d	Mid-Stage Embryo
Crocodylus moreletii	CSUC 1633e	Mid-Stage Embryo
Crocodylus moreletii	CSUC 1633f	Mid-Stage Embryo
Crocodylus moreletii	CSUC 1633g	Mid-Stage Embryo
Crocodylus moreletii	CSUC 1633h	Mid-Stage Embryo
Crocodylus moreletii	CSUC 1633i	Mid-Stage Embryo
Crocodylus moreletii	CSUC 1633k	Mid-Stage Embryo
Crocodylus moreletii	CSUC 1633l	Mid-Stage Embryo
Crocodylus moreletii	CSUC 1647	Mid-Stage Embryo
Crocodylus moreletii	CSUC 1617	Late-Stage Embryo
Crocodylus moreletii	CSUC 1633j	Late-Stage Embryo
Crocodylus moreletii	CSUC 1633m	Late-Stage Embryo
Crocodylus moreletii	CSUC 1633n	Late-Stage Embryo
Crocodylus moreletii	CSUC 1633o	Late-Stage Embryo
Crocodylus moreletii	CSUC 1651	Late-Stage Embryo
Crocodylus moreletii	CSUC 1653	Late-Stage Embryo
Crocodylus moreletii	CSUC 2585	Late-Stage Embryo
Crocodylus moreletii	TMM-M-4980	Subadult
Crocodylus moreletii	TMM-M-5491	Subadult
Crocodylus niloticus	BMNH 1910_3_15_1	Hatchling
Crocodylus niloticus	UF 184612	Hatchling
Crocodylus niloticus	UCMP 140795	Subadult

Crocodylus niloticus	UCMP 140796	Subadult
Crocodylus niloticus	MCZ 50302	Adult
Gavialis gengeticus	SAAF A11077	Mid-Stage Embryo
Gavialis gengeticus	BMNH 49.9.6.2	Hatchling
Gavialis gengeticus	BMNH Gavialis J	Hatchling
Gavialis gengeticus	TMM-M-5486	Juvenile
Gavialis gengeticus	TMM-M-5490	Juvenile
Gavialis gengeticus	TMM-M-5485	Subadult
Gavialis gengeticus	TMM-M-5487	Subadult
Gavialis gengeticus	MCZ 33950	Adult
Gavialis gengeticus	MCZ 46551	Adult
Gavialis gengeticus	UF 118998	Adult
Mecistops cataphractus	BMNH 1953.1.11.30	Mid-Stage Embryo
Mecistops cataphractus	BMNH 1953.1.11.31	Mid-Stage Embryo
Mecistops cataphractus	BMNH 1953.1.11.32	Mid-Stage Embryo
Mecistops cataphractus	BMNH 1953.1.11.38	Mid-Stage Embryo
Mecistops cataphractus	BMNH 1953.1.11.33	Late-Stage Embryo
Mecistops cataphractus	BMNH 1908.5.24.4	Hatchling
Mecistops cataphractus	MCZ 54251	Subadult
Mecistops cataphractus	TMM-M-3529	Subadult
Mecistops cataphractus	MCZ 22483	Adult
Osteolaemus tetraspis	ZOT 001	Mid-Stage Embryo
Osteolaemus tetraspis	ZOT 002	Mid-Stage Embryo
Osteolaemus tetraspis	UF 184616	Late-Stage Embryo
Osteolaemus tetraspis	UF 184617	Late-Stage Embryo
Osteolaemus tetraspis	UF 184618	Late-Stage Embryo
Osteolaemus tetraspis	ZOT 003	Late-Stage Embryo
Osteolaemus tetraspis	ZOT 004	Late-Stage Embryo
Osteolaemus tetraspis	BMNH 1912.6.11.1	Hatchling
Osteolaemus tetraspis	BMNH 1971.236	Hatchling
Osteolaemus tetraspis	MCZ 22913	Subadult
Osteolaemus tetraspis	MCZ 17704	Adult
Paleosuchus trigonatus	UF 184619	Late-Stage Embryo
Paleosuchus trigonatus	UF 184620	Late-Stage Embryo
Paleosuchus trigonatus	BMNH 69.5.21.30	Hatchling
Paleosuchus trigonatus	TMM-M-11981	Juvenile
Paleosuchus trigonatus	MCZ 84030	Adult
Tomistoma schlegelii	COTW 1	Late-Stage Embryo
Tomistoma schlegelii	COTW 2	Late-Stage Embryo
Tomistoma schlegelii	COTW 3	Late-Stage Embryo
Tomistoma schlegelii	BMNH 1863.10.4.1	Hatchling
Tomistoma schlegelii	TMM-M-6342	Subadult
Tomistoma schlegelii	TMM-M-6820	Subadult
Tomistoma schlegelii	WI-22-19	Subadult
Tomistoma schlegelii	UCMP 81702	Subadult

Table S1. List of specimen included in analyses and their approximate ontogenetic stage.

Table S2. Dataset composition

Alligatoridae	Ecomorph	Total	Post Hatching	Embryonic	Adult	Subadult	Juvenile	Hatchling	Late-Stage Embryo	Mid-Stage Embryo
Alligator mississippiensis	Moderate	19	13	6	5	3	5	0	2	4
Caiman crocodilus	Blunt	18	15	3	6	5	4	1	1	1
Paleosuchus trigonatus	Moderate	5	2	3	1	0	1	1	2	0
Crocodylidae										
Crocodylus moreletii	Moderate	22	2	20	0	2	0	0	8	12
Crocodylus niloticus	Moderate	5	3	2	1	2	0	2	0	0
Mecistops cataphractus	Slender	9	3	6	1	2	0	1	1	4
Osteolaemus tetraspis	Blunt	11	2	9	1	1	0	2	5	2
Gavialidae										
Gavialis gengeticus	Slender	10	7	3	3	2	2	2	0	1
Tomistoma schlegelii	Slender	8	4	4	0	4	0	1	3	0
Total		107	51	56	18	21	12	10	22	24
		29	17	12	7	6	4	3	6	3
		51	20	31	7	7	6	3	12	16
		27	14	13	4	8	2	4	4	5

Table S2. Ecomorph classification and ontogenetic sampling of species included in geometric morphometric analyses.

Table S3. Estimated landmarks

Landmark	Description
1	Rostral most point of premaxilla along the jaw margin
2	Premaxilla-**Maxilla** sutural contact along the jaw margin
3	**Maxilla**-Jugal sutural contact along the jaw margin
4	**Jugal**-Quadratojugal sutural contact along the jaw margin
5	Caudal most point of the quadratojugal
6	Caudal most point of the squamosal along the lateral edge of the skull table
7	Squamosal-**Postorbital** sutural contact along the lateral edge of the skull table
8	Dorsolateral projection of the skull table / Postorbital into the orbit
9	**Postorbital**-Frontal sutural contact along skull table / inner surface of the orbit
10	Dorsal contact of the **Prefrontal**-Frontal suture on the inner surface of the orbit
11	Rostral most point of the orbit along the lacrimal
12	Caudoventral corner of the orbit along the postorbital bar
13	Dorsal most point of the lateral temporal fenestra (infratemporal fenestra) along the ventral curvature of the Postorbital.
14	Rostroventral most point of the lateral temporal fenestra (infratemporal fenestra)
15	Caudoventral most point of the lateral temporal fenestra (infratemporal fenestra); usually concomitant with the dorsal most point of the Jugal-**Quadratojugal** sutural contact
16	Dorsal most point of the Ectopterygoid-**Pterygoid** sutural contact
17	Caudo-ventral most point of the Pterygoid

Table S3. Descriptions of the fixed landmark positions used in the complete lateral skull analysis. Landmarks were positioned principally on the bolded element when sutural contact was weak. Landmarks which anchored the semi-landmark curves along the dorsal face (1 & 9) and skull table (6 & 8) are bolded.

Table S4. Estimated landmarks

Species	Specimen ID	Age	Estimated landmarks
Alligator mississippiensis	MCZ 61221	Juvenile	16, 17
Alligator mississippiensis	TMM-M-983	Subadult	16, 17
Caiman crocodilus	MCZ 3557	Adult	16, 17
Caiman crocodilus	MCZ 46632	Adult	16, 17
Gavialis gengeticus	TMM-M-5490	Juvenile	16, 17
Gavialis gengeticus	TMM-M-5485	Subadult	16, 17
Gavialis gengeticus	MCZ 46551	Adult	16, 17
Mecistops cataphractus	TMM-M-3529	Subadult	16, 17
Paleosuchus trigonatus	UF 184619	Late-Stage Embryo	10
Paleosuchus trigonatus	UF 184620	Late-Stage Embryo	10
Paleosuchus trigonatus	BMNH 69_5_21_30	Hatchling	10
Paleosuchus trigonatus	TMM-M-11981	Juvenile	16, 17

Table S4. Specimens for which landmarks were unable to be identified and positions were estimated based on the variance of the rest of the dataset. Landmark descriptions can be found in the supplementary methods and figure 1.

Table S5. Correlation between principal components and centroid size (log scale)

	Complete Skull		Dorsal Face		Skull Table	
PC	PCC	P value	PCC	P value	PCC	P value
Comp 1	0.91864	0.00000	**0.79463**	**0.00000**	**0.74015**	**0.00000**
Comp 2	0.23375	0.01748	**0.30706**	**0.00161**	0.12335	0.21448
Comp 3	-0.21751	0.02731	**0.29304**	**0.00266**	0.09749	0.32726
Comp 4	-0.04898	0.62318	**0.24843**	**0.01140**	**-0.27139**	**0.00556**
Comp 5	0.06431	0.51867	0.00072	0.99426	0.02930	0.76891
Comp 6	0.00949	0.92420	-0.06848	0.49187	-0.09614	0.33402
Comp 7	-0.04848	0.62678	-0.04168	0.67596	0.10968	0.27008
Comp 8	0.04526	0.64987	-0.09074	0.36202	0.16736	0.09107
Comp 9	-0.01142	0.90888	-0.14885	0.13347	-0.10887	0.27368
Comp 10	0.06964	0.48458	-0.10286	0.30115	0.02824	0.77708
Comp 11	-0.01382	0.88980	0.05610	0.57354	-0.03901	0.69566
Comp 12	-0.02974	0.76558	0.00629	0.94971	0.04996	0.61624
Comp 13	-0.05611	0.57344	0.02526	0.80003	0.03132	0.75349
Comp 14	0.02664	0.78938	0.02959	0.76672	-0.17215	0.08207
Comp 15	0.02180	0.82701	0.11389	0.25202	-0.12477	0.20922
Comp 16	-0.01304	0.89595	-0.03546	0.72213	-0.03195	0.74871
Comp 17	0.04487	0.65265	0.02608	0.79370	-0.00923	0.92625
Comp 18	0.02942	0.76803	-0.00471	0.96237	-0.13175	0.18466
Comp 19	-0.01412	0.88742	-0.00236	0.98116	-0.03235	0.74566
Comp 20	0.01548	0.87666	0.04308	0.66568	-0.01895	0.84933
Comp 21	0.02883	0.77249	-0.02420	0.80828	-0.04644	0.64134
Comp 22	0.02335	0.81487	-0.01716	0.86340	-0.01312	0.89533
Comp 23	0.04534	0.64930	-0.03026	0.76153	0.01489	0.88130
Comp 24	0.00063	0.99495	-0.01029	0.91781	-0.08883	0.37225
Comp 25	-0.03067	0.75840	0.03691	0.71125	0.00780	0.93765
Comp 26	-0.06803	0.49476	0.00989	0.92105	0.05298	0.59506
Comp 27	-0.00098	0.99218	-0.01504	0.88011	0.09506	0.33950
Comp 28	-0.00829	0.93375	0.04184	0.67473	-0.03932	0.69330
Comp 29	0.00807	0.93548	0.02912	0.77028	-0.00282	0.97741
Comp 30	0.02673	0.78867	0.00597	0.95229	0.06249	0.53062
Comp 31	0.02978	0.76526	-0.02435	0.80714	-0.08530	0.39159
Comp 32	0.03875	0.69758	-0.05497	0.58132	0.02365	0.81258
Comp 33	0.03022	0.76185	0.03364	0.73589	-0.02453	0.80573
Comp 34	0.02216	0.82417	-0.05749	0.56405	-0.11370	0.25279
Comp 35	-0.01497	0.88068	0.00669	0.94652	-0.04886	0.62403
Comp 36	-0.00301	0.97593	-0.02791	0.77960	-0.01381	0.88986

Comp 37	-0.01227	0.90208	-0.03386	0.73417	-0.01425	0.88636
Comp 38	-0.03423	0.73139	-0.04562	0.64725	0.05720	0.56601
Comp 39	0.00189	0.98489	0.03935	0.69314	-0.00234	0.98129
Comp 40	-0.04759	0.63308	**-0.40727**	**0.00002**	0.12990	0.19093
Comp 41	0.01562	0.87554				
Comp 42	-0.00316	0.97470				
Comp 43	0.01422	0.88660				
Comp 44	-0.02604	0.79404				
Comp 45	0.00325	0.97402				
Comp 46	-0.01151	0.90815				
Comp 47	0.00127	0.98987				
Comp 48	0.00266	0.97876				
Comp 49	0.02626	0.79235				
Comp 50	-0.01297	0.89651				
Comp 51	0.01455	0.88401				
Comp 52	-0.01730	0.86231				
Comp 53	-0.00662	0.94705				
Comp 54	-0.01600	0.87256				
Comp 55	0.02296	0.81793				
Comp 56	-0.00226	0.98191				
Comp 57	0.00979	0.92183				
Comp 58	-0.02460	0.80516				
Comp 59	-0.01111	0.91133				
Comp 60	-0.01816	0.85553				
Comp 61	-0.00736	0.94116				
Comp 62	0.14102	0.15537				

Table S5. Pearson's correlation coefficients (PCC) and significance values for correlation tests among principal components and size of specimens (log scale).

Table S6. Shape differences among ecomorphs across ontogeny for complete lateral skull

Mid-skeletal period embryos

	Df	SS	MS	R sq	F	Z	P-value	Corrected P-value
Among Ecomorphs	2	0.028467	0.014234	0.14485	1.7785	1.3027	0.108	0.108
Residuals	21	0.168064	0.008003	0.85515				
Total	23	0.196532						

Late-skeletal period embryos

	Df	SS	MS	R sq	F	Z	P-value	Corrected P-value
Among Ecomorphs	2	0.052032	0.026016	0.36148	5.378	3.4311	**0.002**	**0.008**
Residuals	19	0.091912	0.004838	0.63852				
Total	21	0.143944						

Hatchlings

	Df	SS	MS	R sq	F	Z	P-value	Corrected P-value
Among Ecomorphs	2	0.121667	0.060833	0.69958	8.1503	2.2269	**0.018**	**0.036**
Residuals	7	0.052248	0.007464	0.30042				
Total	9	0.173914						

Juveniles

	Df	SS	MS	R sq	F	Z	P-value	Corrected P-value
Among Ecomorphs	2	0.165689	0.082845	0.78115	16.062	3.571	**0.003**	**0.009**
Residuals	9	0.046421	0.005158	0.21885				
Total	11	0.212111						

Subadults

	Df	SS	MS	R sq	F	Z	P-value	Corrected P-value
Among Ecomorphs	2	0.149528	0.074764	0.64111	16.077	4.3802	**0.001**	**0.006**
Residuals	18	0.083706	0.00465	0.35889				
Total	20	0.23323						

Adults

	Df	SS	MS	R sq	F	Z	P-value	Corrected P-value
Among Ecomorphs	2	0.097703	0.048851	0.63437	9.5424	3.4684	**0.001**	**0.006**
Residuals	11	0.056313	0.005119	0.36563				
Total	13	0.154016						

Table S6. Summary of results of P-ANOVA on effect of ecomorph on mean shape within each ontogenetic period. Mid-skeletal period embryos are not significantly different, but all other periods of development show significant differences.

Table S7. Shape differences among ecomorphs across ontogeny for dorsal face curve

Mid-skeletal period embryos

	Df	SS	MS	R sq	F	Z	P-value	Corrected P-value
Among Ecomorphs	2	0.014359	0.00718	0.1932	2.5145	1.5743	0.065	0.065
Residuals	21	0.059962	0.002855	0.8068				
Total	23	0.074321						

Late-skeletal period embryos

	Df	SS	MS	R sq	F	Z	P-value	Corrected P-value
Among Ecomorphs	2	0.02081	0.010405	0.444	7.5864	3.2612	**0.001**	**0.006**
Residuals	19	0.026059	0.001372	0.556				
Total	21	0.046869						

Hatchlings

	Df	SS	MS	R sq	F	Z	P-value	Corrected P-value
Among Ecomorphs	2	0.007156	0.003578	0.62289	5.7811	2.6212	**0.001**	**0.006**
Residuals	7	0.004332	0.000619	0.37711				
Total	9	0.011488						

Juveniles

	Df	SS	MS	R sq	F	Z	P-value	Corrected P-value
Among Ecomorphs	2	0.015111	0.007555	0.71789	11.451	3.9711	**0.001**	**0.006**
Residuals	9	0.005938	0.00066	0.28211				
Total	11	0.021049						

Subadults

	Df	SS	MS	R sq	F	Z	P-value	Corrected P-value
Among Ecomorphs	2	0.018117	0.009058	0.47105	8.0147	3.5751	**0.001**	**0.006**
Residuals	18	0.020344	0.00113	0.52895				
Total	20	0.038461						

Adults

	Df	SS	MS	R sq	F	Z	P-value	Corrected P-value
Among Ecomorphs	2	0.013357	0.006679	0.55641	6.8987	2.9582	**0.002**	**0.006**
Residuals	11	0.010649	0.000968	0.44359				
Total	13	0.024006						

Table S7. Summary of results of P-ANOVA on effect of ecomorph on mean shape within each ontogenetic period for the dorsal face curve only dataset. Mid-skeletal period embryos are not significantly different, but all other periods of development show significant differences.

Table S8. Shape differences among ecomorphs across ontogeny for skull table curve

Mid-skeletal period embryos

	Df	SS	MS	R sq	F	Z	P-value	Corrected P-value
Among	2	0.029644	0.014822	0.4036	7.1058	2.9195	**0.002**	**0.012**
Residuals	21	0.043805	0.002086	0.5964				
Total	23	0.073449						

Late-skeletal period embryos

	Df	SS	MS	R sq	F	Z	P-value	Corrected P-value
Among	2	0.002151	0.001076	0.13745	1.5138	0.9534	0.175	0.356
Residuals	19	0.0135	0.000711	0.86255				
Total	21	0.015651						

Hatchlings

	Df	SS	MS	R sq	F	Z	P-value	Corrected P-value
Among	2	0.002265	0.001133	0.13406	0.5418	-0.625	0.72	0.72
Residuals	7	0.014632	0.00209	0.86594				
Total	9	0.016897						

Juveniles

	Df	SS	MS	R sq	F	Z	P-value	Corrected P-value
Among	2	0.004573	0.002286	0.33036	2.22	1.368	0.102	0.356
Residuals	9	0.009269	0.00103	0.66964				
Total	11	0.013841						

Subadults

	Df	SS	MS	R sq	F	Z	P-value	Corrected P-value
Among	2	0.006887	0.003444	0.27865	3.4766	1.9665	0.02	0.1
Residuals	18	0.01783	0.000991	0.72135				
Total	20	0.024717						

Adults

	Df	SS	MS	R sq	F	Z	P-value	Corrected P-value
Among	2	0.005802	0.002901	0.26125	1.945	1.2475	0.089	0.356
Residuals	11	0.016407	0.001492	0.73875				
Total	13	0.022209						

Table S8. Summary of results of P-ANOVA on effect of ecomorph on mean shape within each ontogenetic period for the skull table curve only dataset. Mid-skeletal period embryos are the only period of ontogeny to show significant differences, with pairwise comparisons revealing moderate ecomorph forms are the only distinct group (likely due to better sampling of earlier ontogenetic stages of moderate ecomorph species).

mparison of regression models with multiple change points for complete lateral sl

Complete Lateral Skull

Model	Breakpoint Lower	Breakpoint Mean	Breakpoint Upper			Ratio
No Break	-	-	-	-63.2	9.5	**6.65**
Common Beakpoint	2.697	2.95	3.22	-33.8	7.5	4.51
Species Specific Breakpoints	1.991	2.398	2.678	0	0	-
Ecomorph Specific Breakpoints	2.1476	2.398	2.935	-13.5	6.6	2.05

Dorsal Face Curve

Model	Breakpoint Lower	Breakpoint Mean	Breakpoint Upper			Ratio
No Break	-	-	-	-62.4	8.5	**7.34**
Common Beakpoint	1.7488	1.916	2.055	-16.7	9.3	1.80
Species Specific Breakpoints	1.49696	1.88	2.273	0	0	-
Ecomorph Specific Breakpoints	1.8756	2.219	2.472	-8.3	4.6	1.80

Skull Table Curve

Model	Breakpoint Lower	Breakpoint Mean	Breakpoint Upper			Ratio
No Break	-	-	-	-36	5.8	**6.21**
Common Beakpoint	2.044	2.5026	2.876	-0.4	1.3	0.31
Species Specific Breakpoints	2.046	2.5218	2.943	-1	0.9	1.11
Ecomorph Specific Breakpoints	2.1047	2.4506	2.861	0	0	-

Table S9. Comparison of regression models with or without breakpoints and sp ecies or ecomorph classification as predictors. The existence of a break point in lateral skull shape was assessed using regression of the common allometric co mponent (CAC) against centroid size (log scaled) for the complete lateral skull, dorsal face curve, and skull table curve datasets. Model comparison revealed th

at allowing for a breakpoint was significantly preferred to no break (**Δ**ELPD:**Δ**SE > 5) across all sets of landmarks, with species and ecomorph specific trajectorie s being slightly better fits. The mean breakpoint and lower and upper confidenc e interval bounds demonstrate that a shift occurs at the upper size of embryos.

Table S10. Differences in ontogenetic trajectories - complete skull

Total Dataset

	Df	SS	MS	R sq	F	Z	P-value	Corrected P-value
Size	1	2.3731	2.3732	0.6764	305.1262	6.0898	**0.001**	**0.009**
Ecomorph	2	0.3192	0.1596	0.0910	20.5210	6.2170	**0.001**	**0.009**
Size:Ecomorph	2	0.0615	0.0308	0.0175	3.9559	3.3951	**0.002**	**0.009**
Residuals	97	0.7544	0.0078	0.2150				
Total	102	3.5083						

	Blunt	Moderate	Slender
Blunt	-	0.175	0.112
Moderate	0.22525	-	**0.009**
Slender	0.27652	**0.34884**	-

Embryonic development only

	Df	SS	MS	R sq	F	Z	P-value	Corrected P-value
Size	1	0.1892	0.1892	0.4287	38.1287	5.5385	**0.001**	**0.009**
Ecomorph	2	0.0323	0.0161	0.0731	3.2513	3.3122	**0.001**	**0.009**
Size:Ecomorph	2	0.0214	0.0107	0.0485	2.1564	2.1402	**0.021**	**0.028**
Residuals	40	0.1985	0.0050	0.4497				
Total	45	0.4414						

	Blunt	Moderate	Slender
Blunt	-	0.637	0.513
Moderate	0.58578	-	**0.024**
Slender	0.87127	**0.68107**	-

Post-hatching growth only

	Df	SS	MS	R sq	F	Z	P-value	Corrected P-value
Size	1	0.3308	0.3308	0.3322	64.8613	5.3284	**0.001**	**0.009**
Ecomorph	2	0.3830	0.1915	0.3846	37.5417	5.7292	**0.001**	**0.009**
Size:Ecomorph	2	0.0219	0.0110	0.0220	2.1504	2.3014	**0.014**	**0.028**
Residuals	51	0.2601	0.0051	0.2612				
Total	56	0.9959						

	Blunt	Moderate	Slender
Blunt	-	0.513	0.24
Moderate	0.43127	-	0.144
Slender	0.63018	0.58706	-

Table S10. Summary of results of P-ANOVA on allometric differences among ecomorphs for the complete skull dataset. Tests were performed on the total sample, embryos only, and post-hatching specimens only to assess whether trends differed across the major breakpoint recovered in the dataset (table S9). Results of pairwise comparisons are shown on the right side with angular differences in slope and p-value are shown in lower and upper halves, respectively.

Table S11. Differences in ontogenetic trajectories - dorsal face curve

Total Dataset

	Df	SS	MS	R sq	F	Z	P-value	Corrected P-value
Size	1	0.1991	0.1991	0.4394	99.0717	5.3545	**0.001**	**0.009**
Ecomorph	2	0.0454	0.0227	0.1001	11.2892	4.4461	**0.001**	**0.009**
Size:Ecomorph	2	0.0137	0.0069	0.0303	3.4131	2.4039	**0.008**	**0.028**
Residuals	97	0.1949	0.0020	0.4302				
Total	102	0.4530						

	Blunt	Moderate	Slender
Blunt	-	0.192	0.072
Moderate	0.48744	-	**0.036**
Slender	0.66489	**0.47434**	-

Embryonic development only

	Df	SS	MS	R sq	F	Z	P-value	Corrected P-value
Size	1	0.0803	0.0803	0.5049	50.4058	4.4756	**0.001**	**0.009**
Ecomorph	2	0.0111	0.0055	0.0697	3.4798	2.4733	**0.007**	**0.028**
Size:Ecomorph	2	0.0039	0.0020	0.0247	1.2327	0.6091	0.288	0.288
Residuals	40	0.0637	0.0016	0.4007				
Total	45	0.1590						

	Blunt	Moderate	Slender
Blunt	-	0.484	0.484
Moderate	0.62747	-	0.332
Slender	0.76126	0.41838	-

Post-hatching growth only

	Df	SS	MS	R sq	F	Z	P-value	Corrected P-value
Size	1	0.0259	0.0259	0.2295	29.8696	4.5494	**0.001**	**0.009**
Ecomorph	2	0.0384	0.0192	0.3403	22.1455	5.4209	**0.001**	**0.009**
Size:Ecomorph	2	0.0043	0.0022	0.0383	2.4919	1.9477	**0.019**	**0.038**
Residuals	51	0.0443	0.0009	0.3919				
Total	56	0.1130						

	Blunt	Moderate	Slender
Blunt	-	0.420	0.245
Moderate	0.65827	-	0.189
Slender	0.96342	0.89099	-

Table S11. Summary of results of P-ANOVA on allometric differences among ecomorphs for the dorsal face curve dataset. Tests were performed on the total sample, embryos only, and post-hatching specimens only to assess whether trends differed across the major breakpoint recovered in the dataset (table S9). Results of pairwise comparisons are shown on the right side with angular differences in slope and p-value are shown in lower and upper halves, respectively.

Table S12. Differences in ontogenetic trajectories - skull table curve

Total Dataset

	Df	SS	MS	R sq	F	Z	P-value	Corrected P-value
Size	1	0.2403	0.2402	0.4717	107.8245	4.4867	**0.001**	**0.009**
Ecomorph	2	0.0476	0.0238	0.0935	10.6851	3.5862	**0.001**	**0.009**
Size:Ecomorph	2	0.0053	0.0027	0.0105	1.1952	0.6413	0.276	0.585
Residuals	97	0.2161	0.0022	0.4244				
Total	102	0.5093						

	Blunt	Moderate	Slender
Blunt	-	0.644	0.900
Moderate	0.25126	-	0.063
Slender	0.24208	0.31235	-

Embryonic development only

	Df	SS	MS	R sq	F	Z	P-value	Corrected P-value
Size	1	0.0459	0.0459	0.3647	28.9258	3.7706	**0.001**	**0.009**
Ecomorph	2	0.0084	0.0042	0.0665	2.6363	1.7039	0.04	0.18
Size:Ecomorph	2	0.0081	0.0041	0.0646	2.5630	1.6989	0.036	0.18
Residuals	40	0.0634	0.0016	0.5043				
Total	45	0.1257						

	Blunt	Moderate	Slender
Blunt	-	0.996	0.996
Moderate	0.97494	-	0.232
Slender	0.98334	0.65409	-

Post-hatching growth only

	Df	SS	MS	R sq	F	Z	P-value	Corrected P-value
Size	1	0.0019	0.0019	0.0223	1.4399	0.8421	0.195	0.585
Ecomorph	2	0.0124	0.0062	0.1475	4.7553	2.6859	**0.002**	**0.012**
Size:Ecomorph	2	0.0033	0.0016	0.0392	1.2645	0.6810	0.249	0.585
Residuals	51	0.0665	0.0013	0.7910				
Total	56	0.0841						

	Blunt	Moderate	Slender
Blunt	-	0.900	0.996
Moderate	1.57365	-	0.996
Slender	0.81628	1.25518	-

Table S12. Summary of results of P-ANOVA on allometric differences among ecomorphs for the skull table curve dataset. Tests were performed on the total sample, embryos only, and post-hatching specimens only to assess whether trends differed across the major breakpoint recovered in the dataset (table S9). Results of pairwise comparisons are shown on the right side with angular differences in slope and p-value are shown in lower and upper halves, respectively.